

University of Louisville

ThinkIR: The University of Louisville's Institutional Repository

Electronic Theses and Dissertations

5-2007

Carbon-sulfur bond formation via alkene addition to an oxidized ruthenium-thiolate.

Kiran B. Venna 1974-
University of Louisville

Follow this and additional works at: <https://ir.library.louisville.edu/etd>

Recommended Citation

Venna, Kiran B. 1974-, "Carbon-sulfur bond formation via alkene addition to an oxidized ruthenium-thiolate." (2007). *Electronic Theses and Dissertations*. Paper 1490.
<https://doi.org/10.18297/etd/1490>

This Master's Thesis is brought to you for free and open access by ThinkIR: The University of Louisville's Institutional Repository. It has been accepted for inclusion in Electronic Theses and Dissertations by an authorized administrator of ThinkIR: The University of Louisville's Institutional Repository. This title appears here courtesy of the author, who has retained all other copyrights. For more information, please contact thinkir@louisville.edu.

**CARBON-SULFUR BOND FORMATION VIA ALKENE
ADDITION TO AN OXIDIZED RUTHENIUM-THIOLATE**

By

KIRAN VENNA

A Thesis Submitted to the Faculty of the Graduate School
of the University of Louisville
in Partial Fulfillment of the Requirements for the Degree of

MASTER OF SCIENCE

Department of Chemistry
University of Louisville
Louisville, Kentucky

May 2007

**CARBON-SULFUR BOND FORMATION VIA ALKENE
ADDITION TO AN OXIDIZED RUTHENIUM-THIOLATE**

By

Kiran Venna
M.S. Nagarjuna University, 1998

May 2007

Advisor: Dr. Craig A. Grapperhaus

Dr. Mark E. Noble

Dr. Frank P. Zamborini

Dr. William Dean

DEDICATION

This thesis is dedicated to my parents Anjali Devi and Madhusudhan Rao, to my brother and sister Vardhan Rao and Sunanda, and to my wife Sarika.

ACKNOWLEDGMENTS

I would like to thank my advisor Dr. Craig A. Grapperhaus for mentoring me over the past several years. I am very grateful for his guidance and patience. Being a part of his group has helped me develop as a chemist and analytical thinker. I am indebted to him for all the knowledge and experience I gained while working under his supervision.

I would also like to thank several of the faculty at University of Louisville for their assistance over the past few years. I would like to express my sincere gratitude to my committee members Dr. Noble and Dr. Zamborini for their advice. In addition, I also would like to thank Dr. William Dean for his time in evaluating my thesis. Special thanks to Dr. Mark Mashuta for his X-ray expertise and Dr. Neal Stolowich for the help with NMR collection. I would also like to thank Dr. Mona Zady, who has helped me tremendously as my senior instructor for teaching labs.

I would like to specially thank my lab mate Martin O'Toole for his support to me throughout my graduation years. My life as a graduate student would have been unbearable without my fellow group members and friends; Majda Kreso, Laura Haysley, Kagna Ouch and Ceasar Masitas. I am grateful for their support and their friendship..

Finally, I would like to thank my family. I thank my wonderful parents who made all of my dreams possible and stood behind my every decision. I thank my brother and sister, Vardhan and Sunanda, for believing in me and encouraging me. I would like to thank my wife Sarika, who has been great support to me in every possible way.

ABSTRACT

Carbon-sulfur bond formation via alkene addition to an oxidized ruthenium-thiolate

Kiran Venna, M.S., Nagarjuna University

Chair Advisory Committee: Dr. Craig A. Grapperhaus

May, 2007

This thesis reports the reactivity of the trithiolato Ru complex PPN[Ru(DPPBT)₃] (DPPBT = 2-diphenylphosphinobenzenethiolate) (**1a**) with alkenes upon oxidation. Complex **1a** in acetonitrile shows two redox events at -345 mV and +455 mV in the square wave voltammogram. Bulk oxidation at a holding potential of +100 mV yields [tris(2-(diphenylphosphino)thiaphenolato)ruthenium(III)], (**1b**). During oxidation, the absorption bands at 540 nm, 797 nm and 1041 nm grow in intensity while there is a decrease in the absorption band at 435 nm. A plot of charge versus time during bulk electrolysis shows a total coulometric charge of 1.14 electron equivalent. The square wave voltammogram is not effected by this oxidation. Further oxidation by one electron in the presence of ethylene at a holding potential of +620 mV yields [(ethane-1,2-diylbis(thio-2,1-phenylene)diphenylphosphine)ruthenium(II)] hexafluorophosphate, (**2a**). During oxidation the absorption bands at 540 nm, 797 nm and 1041 nm decrease in intensity. Complex **2a** displays a single redox couple at +804 mV. The +ESI-MS of **2a** shows a parent ion peak at m/z = 1009.1013 amu. The ³¹P NMR spectrum of **2a** shows

chemical shift values of $\delta_1 = 61.0$ ppm, $\delta_2 = 40.3$ ppm, $\delta_3 = 37.5$ ppm with coupling constants of $J_{12} \approx J_{13} \approx 30$ Hz and $J_{23} = 304$ Hz. Complex **2a** can be oxidized at a holding potential of +1000 mV to yield [(ethane-1,2-diylbis(thio-2,1-phenylene)diphenyl phosphine)ruthenium(III)] hexafluorophosphate, (**2b**). The EPR of **2b** displays a rhombic signal with $g_1 = 2.09$, $g_2 = 2.03$, $g_3 = 2.04$. Oxidation of **1b** in the presence of alkenes including 1-hexene, styrene, cyclohexene, and norbornene yield products similar to **2a**. Each of these products can be oxidized to an analogue of **2b**. Complex **2a** can also be prepared, as the bromide salt, from **1a** and 1,2-dibromoethane. The complex [(ethane-1,2-diylbis(thio-2,1-phenylene)diphenylphosphine)ruthenium(II)] bromide crystals as thin yellow plates in the monoclinic space group $P2_1/c$ with unit cell dimensions of $a = 10.2565(9)$ Å, $b = 13.2338(12)$ Å, $c = 38.325(3)$ Å, and $\beta = 93.3960(10)^\circ$.

TABLE OF CONTENTS

	PAGE
ACKNOWLEDGMENTS	iv
ABSTRACT	v
LIST OF FIGURES	ix
LIST OF TABLES	xii
CHAPTER	
I. INTRODUCTION	1
II. EXPERIMENTAL METHODS	7
Materials and Physical Methods	7
Electrochemical Syntheses.....	9
Chemical Synthesis.....	12
III. RESULTS AND DISCUSSION.....	14
IV. CONCLUSIONS.....	44
REFERENCES	50
LIST OF APPENDICES	53
APPENDIX A: Tables and Figure for Crystallographic Data.....	54
APPENDIX B: Electrochemistry.....	61
APPENDIX C: UV-visible Spectroscopy.....	67
APPENDIX D: EPR Spectroscopy.....	71
APPENDIX E: NMR Spectroscopy.....	74
APPENDIX F: Mass Spectroscopy	78

CURRICULUM VITAE.....82

LIST OF FIGURES

FIGURE		PAGE
III-1	Square wave voltammogram of 1a in acetonitrile	21
III-2	Plot of charge versus time acquired during oxidation of 1a to 1b	22
III-3	Electronic spectra obtained during oxidation of 1a to 1b	23
III-4	Plot of charge versus time acquired during oxidation of 1b to 2a	24
III-5	Electronic spectra obtained during oxidation of 1b to 2a	25
III-6	Square wave voltammogram of 2a in acetonitrile	26
III-7	Comparison of square wave voltammogram of 1b and 2a	27
III-8	Plot of charge versus time acquired during oxidation of 2a to 2b	29
III-9	Electronic spectra obtained during oxidation of 2a to 2b	30
III-10	+ESI-MS of 2a in acetonitrile.....	31
III-11	³¹ P NMR spectrum of 2a in deuterated acetonitrile.....	32
III-12	EPR spectrum of 2b	34
III-13	An ORTEP diagram of the cation of 2a with partial atom labeling scheme.....	42
A-3	An ORTEP diagram of the cation of 2a with full atom labeling scheme.....	60
B-1	Square wave voltammogram of 3a	62
B-2	Square wave voltammogram of 4a	62
B-3	Square wave voltammogram of 5a	63

B-4	Square wave voltammogram of 6a	63
B-5	Square wave voltammogram of 2a (chemically generated)	64
B-6	Square wave voltammogram of 3b	64
B-7	Square wave voltammogram of 4b	65
B-8	Square wave voltammogram of 5b	65
B-9	Square wave voltammogram of 6b	66
C-1	Electronic spectra obtained during oxidation of 1b to 3a	68
C-2	Electronic spectra obtained during oxidation of 1b to 4a	68
C-3	Electronic spectra obtained during oxidation of 1b to 5a	69
C-4	Electronic spectra obtained during oxidation of 3a to 3b	69
C-5	Electronic spectra obtained during oxidation of 4a to 4b	70
C-6	Electronic spectra obtained during oxidation of 5a to 5b	70
D-1	EPR spectrum of 3b	72
D-2	EPR spectrum of 4b	72
D-3	EPR spectrum of 5b	73
D-4	EPR spectrum of 6b	73
E-1	³¹ P NMR spectrum of 3a	75
E-2	³¹ P NMR spectrum of 4a-I in deuterated acetonitrile	75
E-3	³¹ P NMR spectrum of 4a-II in deuterated acetonitrile	76
E-4	³¹ P NMR spectrum of 5a in deuterated acetonitrile	76
E-5	³¹ P NMR spectrum of 6a in deuterated acetonitrile	77
F-1	+ESI-MS of 3a in acetonitrile	79
F-2	+ESI-MS of 4a in acetonitrile	79

F-3	+ESI-MS of 5a in acetonitrile.....	80
F-4	+ESI-MS of 6a in acetonitrile.....	80
F-5	+ESI-MS of 2a (chemically generated) in acetonitrile.....	81

LIST OF TABLES

CHAPTER		PAGE
III-1	Square wave voltammogram, +ESI-MS, and ³¹ P NMR of 3a , 4a , 5a , and 6a	36
III-2	Electronic absorption maximum and EPR g-values of 3b , 4b , 5b , and 6b	38
III-3	Comparison of square wave voltammogram, +ESI-MS, and ³¹ P NMR of chemically and electrochemically generated 2a	40
A-1	Experimental data for the X-ray crystal structure of 2a	55
A-2	Bond lengths [Å] and bond angles [°] for 2a	56

CHAPTER I

INTRODUCTION

Sulfenyl radicals, also commonly referred to as thiyl radicals, are organosulfur compounds with an unpaired electron on sulfur and the general formula $RS\cdot$.¹ These $RS\cdot$ thiyl radicals can be generally generated chemically with one electron oxidants or electrochemically by applying a sufficiently positive potential. Additionally, pulse radiolysis has been extensively used for generation of thiyl radicals for reactivity studies. Finally, thiyl radicals can also be generated by photolysis of disulfides with ultraviolet radiation or by the oxidation of transition metal thiolates.²

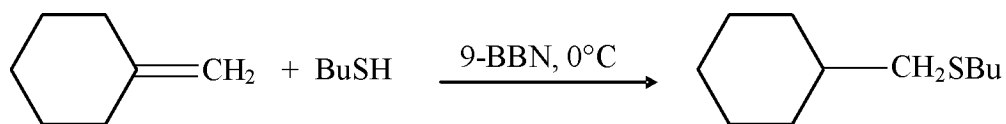
Once generated, thiyl radicals can be recognized by spin trapping techniques. Important methods to understand radical reactivity include stop flow UV-visible spectroscopy, and rapid freeze quench electron paramagnetic resonance (EPR) spectroscopy.³ EPR is a very important tool for identifying thiyl radicals. However, due to large spin-orbit coupling effects for sulfur, the EPR signal broadens, leading to a decrease in sensitivity of detecting thiyl radicals. Recently, sulfur K-edge X-ray absorption spectroscopy was reported as a useful tool to detect thiyl radicals.⁴ With this method, even EPR silent species can be detected. Apart from these experimental techniques, density functional theory (DFT) studies and correlated *ab initio* studies have also been employed to better understand the electronic structure of thiyl radicals.⁵

The reactivity of thiyl radicals with non-sulfur containing organic compounds typically correspond to one of two major reaction classes. First, thiyl radicals can react

with hydrocarbons in a C-S bond forming reaction. Second, thiyl radicals can abstract hydrogen from unsaturated hydrocarbons and others. The reactivity of $RS\cdot$ thiyl radicals with unsaturated organic compounds has been studied for over five decades.⁶ In 1958, Helmreich and coworkers reported thiyl radical initiated isomerization of cis-alkenes to trans alkenes in a reversible reaction.⁷ Thiyl radical can react with various alkynes in a similar fashion. Abstraction of the hydrogen from a C-H bond by thiyl radical involves formation of a S-H bond. This reaction is not favorable with all the hydrocarbons, since the average C-H bond enthalpy of $98.3 \pm 0.8 \text{ kcal mol}^{-1}$ is greater than that of an average S-H bond, $87 \pm 1 \text{ kcal mol}^{-1}$.⁸ Thus, abstraction of hydrogen generally is favored for activated C-H bonds, such as when an electron withdrawing group is present.

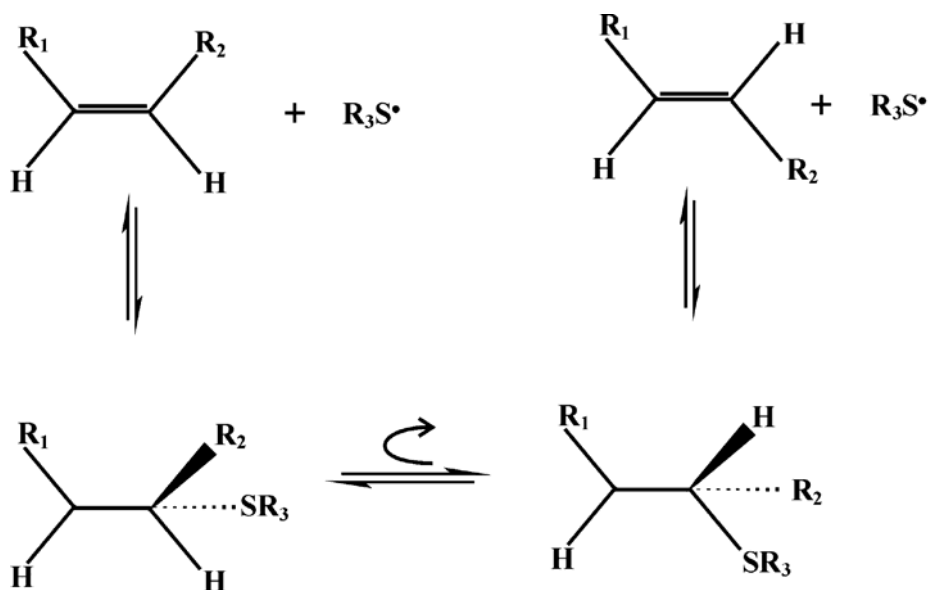
The addition of thiyl radicals to alkene to form C-S bonds was exploited by the Ichinose group for the synthesis of sulfides.⁹ In this reaction, a thiyl radical was generated from butanethiol, with the help of the radical initiator 9-BBN (9-bora-bicyclo [3.3.1.] nonane), and then reacted with methylene cyclohexene, Scheme I-1. From this reaction it is clear that addition of thiyl radicals to alkenes leads to formation of new C-S bond. Apart from the C-S bond formation reaction, thiyl radicals have also been used in the initiation of block polymerization. Very recently a tetrazole derived thiyl radical, which reacts with alkenes with very low selectivity but very high reactivity, has been reported.¹⁰ Due to the high reactivity of above mentioned thiyl radical, it can react with various monomers including vinyl acetate and methyl acrylate in the polymerization to form their respective polymers.

Scheme I-1.



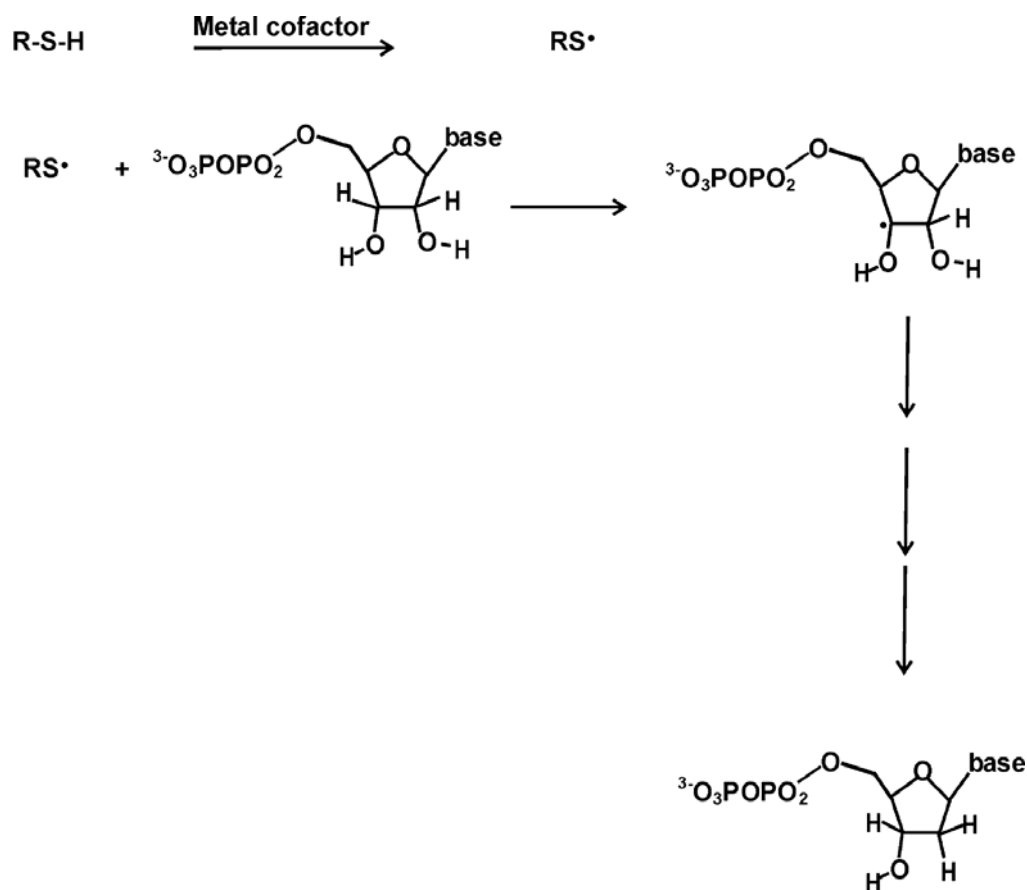
The thiyl radical reactivity seen in organic synthesis has also been utilized by nature in various biological systems. Thiyl radicals have been implicated in the cis-trans isomerization of unsaturated fatty acid in cell membranes, Scheme I-2.¹¹ This isomerization is employed by certain bacteria, including *Pseudomonas putida*, to protect themselves from adverse environments. The thiyl radical attacks the cis double bond of fatty acid present in membranes. This allows rotation around the carbon-carbon bond axis and conversion to a trans-configuration. Subsequent β elimination of the thiyl radical yields the trans isomer. This isomerization reaction is reversible.

Scheme I-2.



A more prominent biological role for thiyl radicals involves hydrogen abstraction. Hydrogen abstraction from a C-H bond by thiyl radicals was prominently studied in ribonucleotide reductases (RNR), an enzyme which plays a major role in the synthesis of DNA. The conversion of the ribonucleotides to deoxyribonucleotides is initiated by a thiyl radical that is generated in various RNR's by metal cofactors. Metal cofactors containing Co, Fe and Mn are known to assist in the oxidation of thiolate to thiyl radicals. The thiyl radical abstracts hydrogen from 3' carbon of the ribose unit, Scheme I-3. Elimination of hydrogen generates a 3' carbon radical and which takes part in further steps and finally rearranges to form a deoxyribose unit.¹²

Scheme I-3.



It is important to note that phenylthiyl radicals are more reactive than the corresponding phenoxy analogues. The phenoxy radical is stabilized by delocalization of the unpaired electron into the phenyl ring. However, for the phenylthiyl radical, the energy of the 3p sulfur orbital is too high for efficient delocalization and the radical is sulfur-centered. Coordination of thiyl radicals to metal ions can influence their stability and reactivity. Metal-coordinated thiyl radicals can be stabilized by delocalization of the unpaired spin onto the metal d-orbitals. Due to this reason reactivity of the metal thiyl will be less when compared to an organic thiyl radical.¹³

Metal-coordinated thiyl radicals are obtained by oxidation of metal thiolates. Attempts to generate and stabilize metal-coordinated thiyl radicals have been reported by various groups.¹³⁻¹⁶ In the absence of any other suitable substrates, they react with themselves to form disulfide bonds. Disulfide bond formation was studied by Triebel and coworkers upon oxidation of $[\text{Fe}(\text{SPh})(\text{CO})(\text{PPh}_3)(\eta\text{-C}_5\text{H}_5)]\text{PF}_6$, which led to the bridged binuclear species $[\text{Fe}(\text{CO})(\text{PPh}_3)(\eta\text{-C}_5\text{H}_5)(\mu\text{-SSPh}_2)]^{2+}$.¹⁷ Oxidation in this case was irreversible. Reversible thiolate centered oxidation was reported by the Wieghardt group in case of $([\text{Ru}^{\text{III}}\text{L}])$, $\text{L} = 1,4,7\text{-tris}(4\text{-tert-butyl-2-mercaptobenzyl})\text{-1,4, 7-triazacyclononane}$ which also yielded disulfide complex.¹⁸

The study of this thesis is to understand the reactivity of metal-coordinated thiyl radicals, generated from oxidation of metallothiolates, towards various alkenes. It is expected that with sufficient steric bulk around the thiyl radical, disulfide formation will be disfavored. Previous results in the Grapperhaus group have shown this to be the case for thiyl radical generated from $[\text{Ru}(\text{DPPBT})_3]$ (DPPBT = 2-diphenylphosphinobenzenethiolate).¹⁹ Further, coordination of the thiyl radical should

reduce the tendency for C-H bond abstraction since the metal ion acts as an electron withdrawing group, thus decreasing the strength of the S-H bond. Thus, we expect the thiyl radical complex $[\text{Ru}(\text{DPPBT})_3]^+$ should favor reactivity with unsaturated hydrocarbons. Previously, $[\text{Ru}(\text{DPPBT})_3]^+$ was shown to react with methyl ketones, presumably as the enol tautomer, to generate C-S bonds.²⁰ As such, $[\text{Ru}(\text{DPPBT})_3]^+$ should show similar reactivity with alkenes to generate dithioethers.

CHAPTER II

EXPERIMENTAL METHODS

Materials and Physical Methods

Chemicals were purchased from available commercial sources (Aldrich, VWR chemicals, TCI, Acros Organic, or Alfa Aesar) and were used as received, unless otherwise specified. Bis(triphenylphosphoranylidene)ammonium chloride (PPNCl) was purchased from Aldrich and was purified by recrystallization from methanol prior to use. Styrene, 1,2-dibromoethane, cyclohexene, and 1-hexene were purchased from Aldrich and used as received. Ethylene gas was purchased from Matheson. The complex [PPN][Ru(DPPBT)₃] (**1a**) was synthesized according to published procedures and was stored in a nitrogen atmosphere dry box.²¹ Deuterated solvents required for NMR experiments were purchased from Cambridge Isotope Laboratories and used without further purification.

All reactions were conducted under anaerobic conditions by using standard Schlenk techniques, unless otherwise specified. All solvents were purchased from VWR chemicals or Aldrich and purified by standard methods.²² All solvents were freshly distilled before use.

NMR spectra were recorded on a Varian 500 MHz spectrometer and referenced to TMS (¹H NMR) or 85% phosphoric acid (³¹P NMR). Electron paramagnetic resonance spectra were collected on a Bruker EMX EPR spectrometer at 77 K in a Suprasil quartz

dewar. Electro-spray Ionization (ESI) mass spectra were recorded at the Mass Spectrometry Application and Collaboration Facility in the Chemistry Department at Texas A&M University.

The X-ray crystal structure of [(ethane-1,2-diylbis(thio-2,1-phenylene)diphenylphosphine)ruthenium(II)] bromide was determined by Dr. Mark Mashuta at the X-ray diffraction laboratory at the University of Louisville. A single crystal of [(ethane-1,2-diylbis(thio-2,1-phenylene)diphenylphosphine)ruthenium(II)] bromide was selected and mounted on a loop. The data was obtained on a Bruker SMART APEX CCD diffractometer. A summary of the data collection as well as the complete bond lengths and bond angles are located in Appendix A.

Electrochemical and spectroelectrochemical experiments were performed in a custom cell designed by E. Böhle of Max-Planck Institute für Bioanorganische Chemie, Mülheim, Germany. The cell has a quartz window with a path length of 0.5 cm and variable temperature jacketed sample holder. The cell was connected to a VWR 1190A chiller that was set at -34 °C, which resulted in temperature of -22 ± 3 °C in the cell. All the measurements were taken at the above mentioned temperature unless noted otherwise. To avoid condensation on the cell during low temperature conditions, the cell holder was placed in a Plexiglas box fitted with Dynasil 4000 quartz windows (Pacific Quartz), through which nitrogen gas was purged. Coulometric and UV-visible measurements were done simultaneously with 10 mL acetonitrile as solvent and 0.1 M tetrabutylammonium hexafluorophosphate (TBAHFP) as supporting electrolyte. Nitrogen was purged in the cell to prevent oxygen diffusion and also to ensure proper solution mixing. For coulometric measurements platinum mesh was used as working electrode with Ag^0/Ag^+

as reference electrode. After each oxidation, the working electrode was changed to a glassy carbon electrode and nitrogen purging was stopped and the square wave voltammogram was recorded.

Electrochemical Syntheses

Electrochemical synthesis of [(ethane-1,2-diylbis(thio-2,1-phenylene)diphenyl phosphine)ruthenium(II)] hexafluorophosphate, **2a:** All manipulations and measurements were performed in a fume hood. To the custom designed spectroelectrochemical cell kept at -22 ± 3 °C, 10 mL of acetonitrile were added along with 0.387 g (0.1 M) of TBAHFP. Next, 0.020 g (0.013 mmol) of [PPN][Ru(DPPBT)₃] (**1a**) was added resulting in an orange colored solution that was kept under nitrogen bubbling for ~15 minutes. To convert **1a** to [tris(2-(diphenylphosphino)thiaphenolato)ruthenium(III)] (**1b**), a potential of +100 mV was applied until the current was reduced to less than 10 μ A. In a typical trial, 1410 mC (1.14 electron equivalent) of charge was produced. During oxidation, the color of the solution changed to brown (λ_{max} (nm) = 540, 797, 1041). The square wave voltammogram showed events at -345 mV and +455 mV.

To the freshly prepared brown solution of **1b**, ethylene gas was bubbled until completion of the reaction, while a potential of +620 mV was applied. During the oxidation, the color of the solution changed to light yellow. After ~1049 mC (0.83 electron equivalent) charge production, the current decayed to less than 10 μ A. The resulting solution contained **2a**. $E_{1/2} = +804$ mV. Electronic absorption: λ_{max} (nm): silent in 400-1100 region. +ESI-MS for C₅₆H₄₆P₃S₃Ru: experimental = 1009.1013 amu, theoretical = 1009.1018 amu.

Electrochemical synthesis of [(ethane-1,2-diylbis(thio-2,1-phenylene)diphenyl phosphine)ruthenium(III)] hexafluorophosphate, 2b: In the custom designed spectroelectrochemical cell, a potential of +1000 mV was applied to a freshly prepared solution of **2a** at -22 ± 3 °C. When the current decayed to less than 10 μ A, oxidation was ceased. A green-colored solution was obtained. A small aliquot was removed via microsyringe and frozen at 77 K in a nitrogen filled EPR tube. $E_{1/2} = +798$ mV. Electronic absorption: λ_{max} (ϵ): 690 nm (3818). EPR: $g = 2.09, 2.03,$ and 2.04 . Samples of **2b** can be reduced to **2a** at an applied potential of +700 mV.

Electrochemical synthesis of [(hexane-1,2-diylbis(thio-2,1-phenylene)diphenyl phosphine)ruthenium(II)] hexafluorophosphate, 3a: Electrochemical synthesis of **3a** is similar to that of **2a**. A solution of **1b** was generated electrochemically as described above. Then, 2.0 mL (16 mmol) of 1-hexene was added and nitrogen gas was purged through the solution during bulk electrolysis at an applied potential of +620 mV. $E_{1/2} = +792$ mV. Electronic absorption: λ_{max} (nm): silent in 400-1100 region. +ESI-MS for $\text{C}_{60}\text{H}_{54}\text{P}_3\text{S}_3\text{Ru}$: experimental = 1065.1655 amu, theoretical = 1065.1643 amu.

Electrochemical synthesis of [(hexane-1,2-diylbis(thio-2,1-phenylene)diphenyl phosphine)ruthenium(III)] hexafluorophosphate, 3b: Complex **3b** was prepared from **3a** in a manner analogous to electrochemical synthesis of **2b** from **2a**. $E_{1/2} = +798$ mV. Electronic absorption: λ_{max} (ϵ): 682 nm (2727). EPR: $g = 2.08, 2.03,$ and 2.02 . Samples of **3b** can be reduced to **3a** at an applied potential of +700 mV.

Electrochemical synthesis of [(phenylethane-1,2-diylbis(thio-2,1-phenylene)diphenyl phosphine)ruthenium(II)] hexafluorophosphate, 4a: Complex **1b** was generated electrochemically as described above. Then, the cell was covered with aluminum foil to

prevent exposure of styrene to light. Using a syringe, 2.0 mL (17 mmol) of styrene was added and the solution was mixed by a nitrogen purge for 5 minutes. The resulting mixture was then oxidized in a manner analogous to electrochemical synthesis of **3a** at an applied potential of +620 mV. $E_{1/2} = +788$ mV. Electronic absorption: λ_{max} (nm): silent in region of 400-1100. +ESI-MS for $\text{C}_{62}\text{H}_{50}\text{P}_3\text{S}_3\text{Ru}$: experimental = 1085.1317 amu, theoretical = 1085.1331 amu.

Electrochemical synthesis of [(phenylethane-1,2-diylbis(thio-2,1-phenylene)diphenyl phosphine)ruthenium(III)] hexafluorophosphate, 4b: Complex **4b** was prepared from **4a** in a manner analogous to electrochemical synthesis of **2b** from **2a**. $E_{1/2} = +808$ mV. Electronic absorption: λ_{max} (ϵ): 692 nm (2181). EPR: $g = 2.09, 2.05, 2.03$. Samples of **4b** can be reduced to **4a** at an applied potential of +700 mV.

Electrochemical synthesis of [(cyclohexane-1,2-diylbis(thio-2,1-phenylene)diphenyl phosphine)ruthenium(II)] hexafluorophosphate, 5a : Complex **1b** was generated electrochemically as mentioned previously. After the generation of **1b**, 2.0 ml (20 mmol) of the cyclohexene was added and the solution was mixed by a nitrogen purge for 5 minutes, then the mixture was oxidized as described for electrochemical synthesis of **3a** at an applied potential of +620 mV. $E_{1/2} = +790$ mV. Electronic absorption: λ_{max} (nm): silent in region of 400-1100. ESI-MS for $\text{C}_{60}\text{H}_{52}\text{P}_3\text{S}_3\text{Ru}$: experimental = 1063.1493 amu, theoretical = 1063.1487 amu.

Electrochemical synthesis of [(cyclohexane-1,2-diylbis(thio-2,1-phenylene)diphenyl phosphine)ruthenium(III)] hexafluorophosphate, 5b: Complex **5b** was electrochemically synthesized from **5a** in a manner analogous to the preparation of **2b** from

2a. $E_{1/2} = +782$ mV. Electronic absorption: λ_{\max} (ϵ): 697 (2545). EPR: $g = 2.09, 2.05, 2.02$. Samples of **5b** can be reduced to **5a** at an applied potential of +700 mV.

Electrochemical synthesis of [(norborene-1,2-diylbis(thio-2,1-phenylene)diphenyl phosphine)ruthenium(II)] hexafluorophosphate, 6a: To a solution of **1b**, generated electrochemically as described above, 0.100 g of norbornene (1.06 mmol) was added and nitrogen purging was done for 15 minutes to ensure proper mixing. The resulting mixture was oxidized as described for **3a** at an applied potential of +620 mV. $E_{1/2} = +824$ mV. Electronic absorption was not determined owing to solubility problems. +ESI-MS for $C_{61}H_{52}P_3S_3Ru$: experimental = 1075.1478 amu, theoretical = 1075.1487 amu.

Electrochemical synthesis of [(norborene-1,2-diylbis(thio-2,1-phenylene)diphenyl phosphine)ruthenium(III)] hexafluorophosphate, 6b: Complex **6b** was synthesized from **6a**, from the method analogous to electrochemical synthesis of **2b** from **2a**. $E_{1/2} = +834$ mV. Electronic absorption was not determined owing to solubility problems. EPR: $g = 2.09, 2.05, 2.03$. Samples of **6b** can be reduced to **6a** at an applied potential of +700 mV.

Chemical Synthesis

[(ethane-1,2-diylbis(thio-2,1-phenylene)diphenyl phosphine)ruthenium(II)] bromide, 2a: To 17 mL of chlorobenzene, 0.092 g (0.061 mmol) of **1a** was added and was stirred for 10 minutes. To the resulting yellow mixture, 0.18 g (0.097 mmol) of 1,2-dibromoethane was added via microsyringe and was left for overnight stirring. The resulting dark red colored solution was filtered through Celite. Diethyl ether layering on the dark red filtrate resulted in yellow crystals. Yield: 0.0354 g (54.7%). $E_{1/2} = +794$ mV.

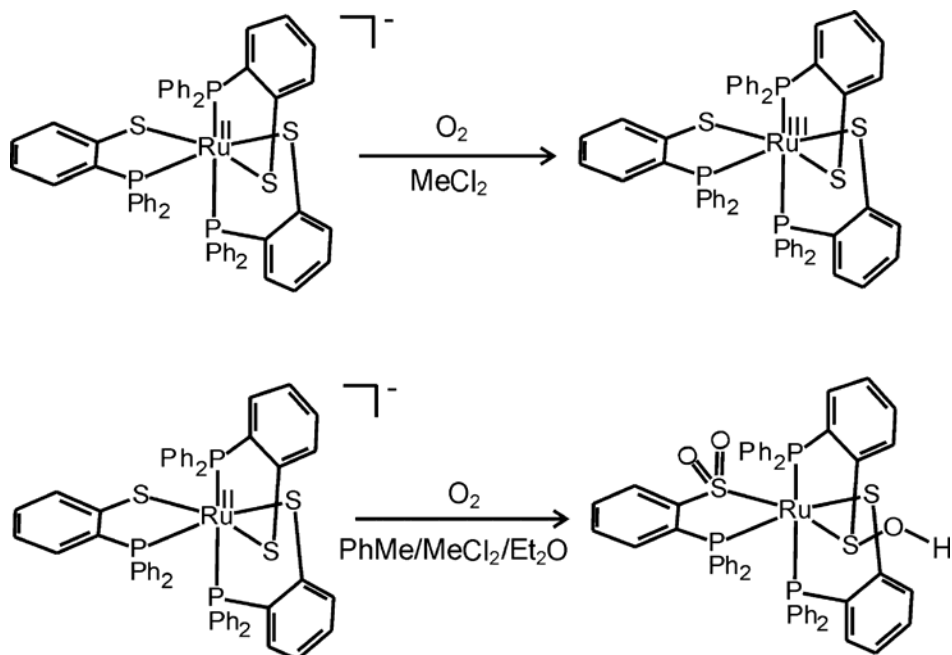
+ESI-MS for $C_{56}H_{46}P_3S_3Ru$: experimental = 1009.1015 amu, theoretical = 1009.1018 amu.

CHAPTER III

RESULTS AND DISCUSSION

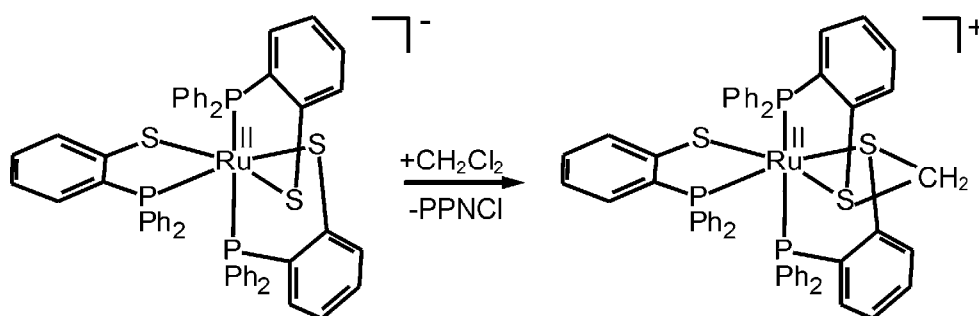
The trithiolate ruthenium complex $[\text{Ru}(\text{DPPBT})_3]^-$ (**1a**) was earlier reported by Dilworth as the triethylammonium, $[\text{HNEt}_3]^+$, salt.²³ In those reports, the oxidation behavior was described as solvent dependent, Scheme III-1. Aerobic oxidation of $[\text{Ru}(\text{DPPBT})_3]^-$ in dichloromethane solution resulted in metal-centered oxidation of Ru(II) to Ru(III), whereas oxidation in a mixture of solvents including toluene, dichloromethane, and diethyl ether showed ligand-centered oxygenation. Unfortunately, the poor solubility of the complex as the triethylammonium salt complicated the study of these reactions by various spectroscopic methods.

Scheme III-1



To overcome the solubility issue and understand the solvent dependence, the bis(triphenylphosphoranylidene)ammonium ([PPN]⁺) salt of [Ru(DPPBT)₃]⁻ was isolated and extensively studied in the Grapperhaus research group.^{19,21,24} Initial studies with the PPN⁺ salt of **1a** in dichloromethane shows C-S bond formation leading to a dithioether product, Scheme III-2, under anaerobic conditions.²¹ The structure of the methylene-bridged dithioether/thiolate complex [Ru(DBBT)₂CH₂](DPPBT)]Cl was confirmed by X-ray crystallography.

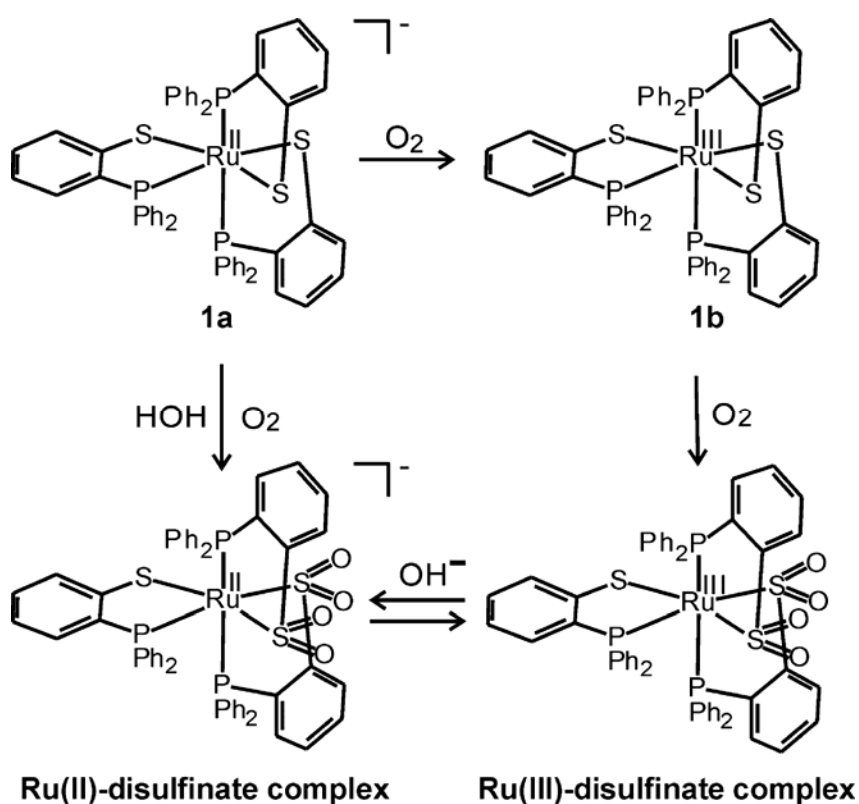
Scheme III-2.



When **1a** was exposed to O₂, a complex series of reactions leading to sulfur oxygenation was observed, Scheme III-3.²⁴ The oxygen reactivity of **1a** was studied by exposing acetonitrile/methanol solution of **1a** to oxygen and monitoring the reaction by UV-visible spectroscopy. Initial dissolution of the **1a** in acetonitrile/methanol resulted in a yellow solution with an absorption band at 435 nm. After initial exposure to oxygen for 1 to 2 hours, the color of the solution changed to brown with stronger bands at 540 nm, 797 nm and 1041 nm. These bands can be readily assigned to the Ru(III)-trithiolate, **1b**. From this result it is evident that initial oxidation is metal-based. Upon prolonged oxidation (i.e. for ~15 hours), the brown colored solution returned to yellow color. The

ESI-MS of the sample shows a peak at $m/z = 1045.0$, which indicates the addition of 4 oxygen atoms to **1b** to yield a disulfinate complex. This disulfinate complex formation was confirmed by IR and X-ray crystallographic investigations. The oxygenation results in a large shift of the Ru(III)/(II) reduction potential and the Ru(II) derivative is isolated.²⁴

Scheme III-3.



To further understand the reactivity of **1a**, electrochemical investigations were undertaken with *in situ* monitoring by UV-visible spectroscopy.¹⁹ The square wave voltammogram of **1a** in acetonitrile shows a pair of redox couples at -345 mV and +455 mV. Bulk oxidation of **1a** at an applied potential of +100 mV was employed to generate

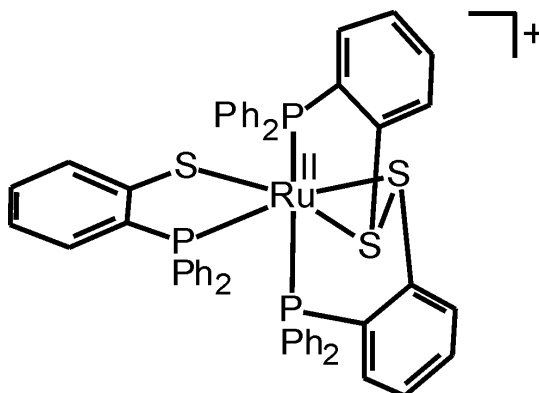
1b. During the bulk oxidation, the color of the solution changed from yellow to brown. Following oxidation, the square wave voltammogram of **1b** showed bands at -345 mV and +455 mV confirming no change in the donor environment. The absorption bands of **1b** are observed at 540 nm, 797 nm, and 1041 nm. In total, the bulk oxidation generated one electron equivalent with a coulometric charge of 945 (± 20) mC for a 1 mM solution. The EPR of **1b** shows a characteristic rhombic signal with g-values of 2.12, 2.06 and 2.04 confirming the presence of Ru(III).

The complex **1b** can be further oxidized by holding a potential more positive than +455 mV couple.¹⁹ Bulk electrolysis of **1b** was done at a holding potential at +620 mV. During oxidation, the absorption bands decrease in intensity and a new band at 850 nm, which is due to an intermediate, grows in intensity. However, the intermediate is short lived and before the one electron process is completed the band is diminished. The square wave voltammogram following oxidation is significantly changed from that of **1a/1b**. This indicates a change in the donor environment has occurred.

The intermediate species upon oxidation of **1b** initially was assigned as a Ru coordinated thiyl radical, **1c**.²⁰ This intermediate is short lived and decays to a proposed Ru(II)-disulfide complex, Scheme III-4.¹⁹ The rate of the decay of thiyl radical to disulfide was studied and it shows a rate constant of 10^{-3} s^{-1} . It is suggested that the coordinated radical couples with a thiolate donor to yield a disulfide radical. Disulfide radicals are good reducing agents and the odd electron is transferred to the metal.¹⁸ The Ru(II)-disulfide product is silent in the electronic spectrum between 400 nm and 1000 nm. The square wave voltammogram of Ru(II)-disulfide product shows a single event at a potential of +806 mV. This is a shift of 1151 mV in the Ru(III)/(II) couple consistent

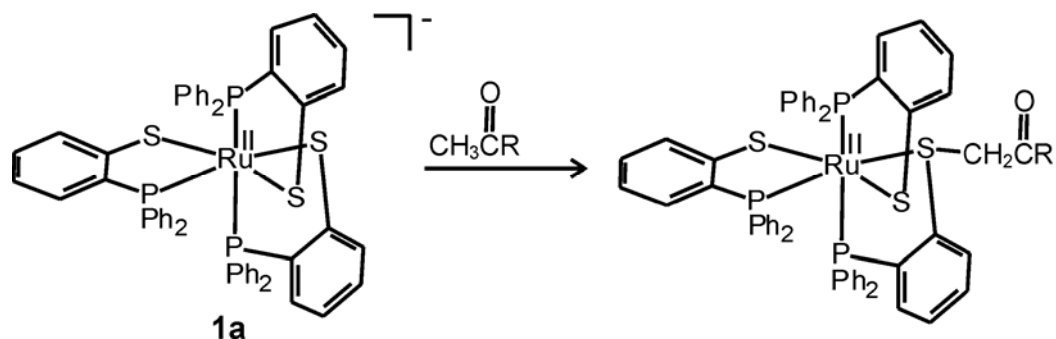
with modification of 2 thiolate donors.^{21,25} The disulfide is not thermally stable and therefore not structurally characterized. The mass spectrum of **1c**, however, shows a parent ion envelope with a signal at $m/z = 981.1$.¹⁹

Scheme III-4.



The slow decay of **1c** suggests it can react with the other suitable targets. Bulk electrolysis of **1b** was done in the presence of methyl ketones at a holding potential of +620 mV. This oxidation involved a 2 electron process, whereas in the presence of acetonitrile this oxidation was a one electron process. Following oxidation, the color of the solution changed to blue. The square wave voltammogram shows a single event at +468 mV assigned as Ru(III)/(II). The +800 mV shift indicates the product is monoalkylated.²⁵ The alkylation was further confirmed by chemical method in which **1a** was reacted with chloroacetone. Crystals of the monoalkylated product were grown and their structure determined by X-ray crystallographic methods. Apart from acetone, bulk oxidation of **1b** was studied with other ketones leading to similar products when a methyl ketone was employed, scheme III-5.²⁰

Scheme III-5.

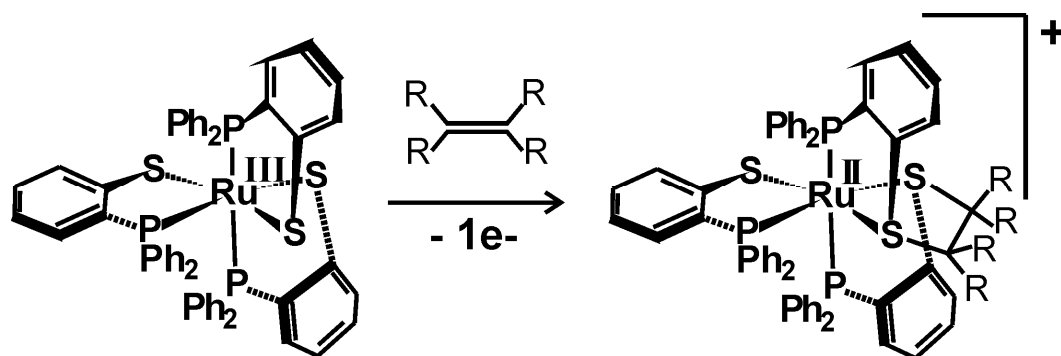


Further evidence suggested the reactivity of **1c** with ketones actually involves the enol tautomer of the ketone. C-S bond formation was earlier reported by Rauchfuss at the sulfide bridge of the ruthenium cluster, $(C_5Me_5)_3RhRu_2S_4(MeCN)^{2+}$ upon reaction with the enol tautomer of acetone.²⁶ A similar approach was shown by Matsumoto group.²⁷ The enol reactivity of ketone towards **1c** gave a scope to study the reactivity of **1a** with various alkenes. Addition of alkenes to oxidized nickel dithiolenes has been previously reported.^{28,29} Very recently, Webster and Goh have reported addition of cis dithiolate $[Cp^*Ru(tpdt)]$ ($Cp^* = \eta^5-C_5Me_5$, $tpdt = \eta^3-S(CH_2-CH_2S^-)_2$) to electrophilic alkenes, like acrylonitrile, upon oxidation.²

The work reported in this thesis is focused on the reactivity of **1c** with a variety of alkenes. To investigate this reactivity, acetonitrile solutions of **1b** were generated by electrochemical oxidation of **1a**. Further bulk electrochemical oxidization to **1c** in the presence of an alkene was then pursued. Various alkenes ranging from the simplest alkene, ethylene, to a bridged alkene, norbornene, were employed to test the robustness of the reactivity of **1c** towards a variety of alkenes. The alkenes employed included 1-hexene, ethylene, norbornene, cyclohexene and styrene. In general, these reactions yield a

Ru(II)-dithioether complex, Scheme III-6. A detailed description for the reaction of **1c** with ethylene is provided below as an example. The complete data for the reaction of **1c** with the alkenes, other than ethylene, is presented in Table III-1 and Table III-2, and figures for the same have been provided in the Appendix.

Scheme III-6.



All bulk electrolysis reactions were conducted in the spectroelectrochemical cell described in Chapter II. The cell was placed in a variable temperature cell holder, connected in a series to a circulating low temperature bath. The temperature of the circulator was set at $-34\text{ }^{\circ}\text{C}$ which resulted in an average temperature of $-22 \pm 3\text{ }^{\circ}\text{C}$ in the cell. In a typical experiment, 10 mL of a 1.13 mM acetonitrile solution of **1a** containing 0.1 M of supporting electrolyte was added to the cell. The supporting electrolyte was tetrabutylammonium hexafluorophosphate (TBAHFP).

Before ethylene addition, a solution of **1b** was freshly prepared by bulk oxidation of **1a**. The charge released during oxidation was recorded and compared to the value predicted based on the mass of **1a** used. This value also provided a benchmark to determine the number of electron equivalents in the subsequent reactions.

To the spectroelectrochemical cell containing 10 mL of acetonitrile, 0.387 g of TBAHFP and 0.020 g of **1a** was added. Nitrogen gas was purged through the solution to remove oxygen and ensure complete dissolution. A glassy carbon working electrode, a platinum wire counter electrode, and a silver reference electrode were placed into the cell. The counter electrode was isolated from the reaction solution by a fritted disk. The square wave voltammogram was recorded. As shown in Figure III-1, complex **1a** displays redox events at -345 mV and +455 mV. After collection of the voltammogram, the glassy carbon working electrode was replaced with a platinum mesh for the bulk electrolysis.

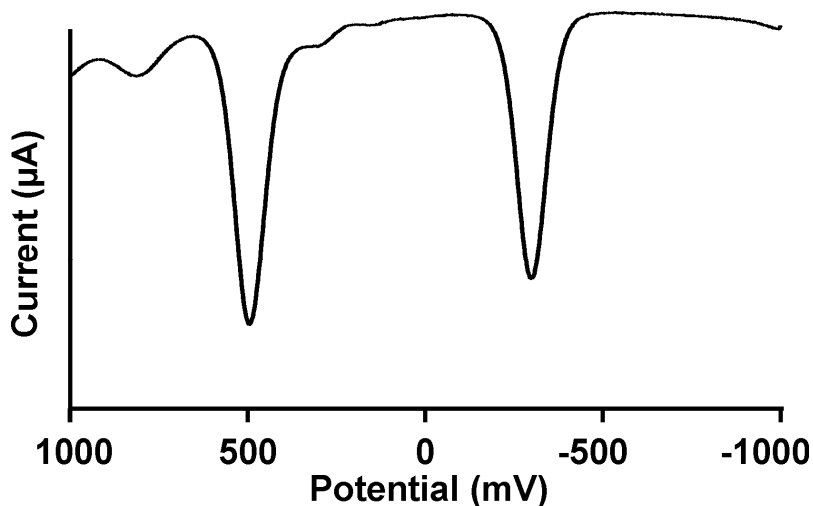


Figure III-1. Square wave voltammogram of **1a** in acetonitrile with 0.1M TBAHFP at -20 °C. Potentials referenced to Ag/AgCl.

Controlled potential oxidation of **1a** to **1b** was accomplished by holding an applied potential of +100 mV. The reaction is assumed to be complete when the current falls to less than 5% of the initial current. In a typical experiment, this occur around 2500

s. A plot of charge versus time, Figure III-2, reveals a total coulometric charge of 1410 mC and this value corresponds to 1.14 electron equivalent oxidation (as per Faraday's law). The square wave voltammogram of the brown product, **1b**, shows the two events again at -345nm and +455nm. This indicates that no significant changes have occurred in the coordination environment around ruthenium.

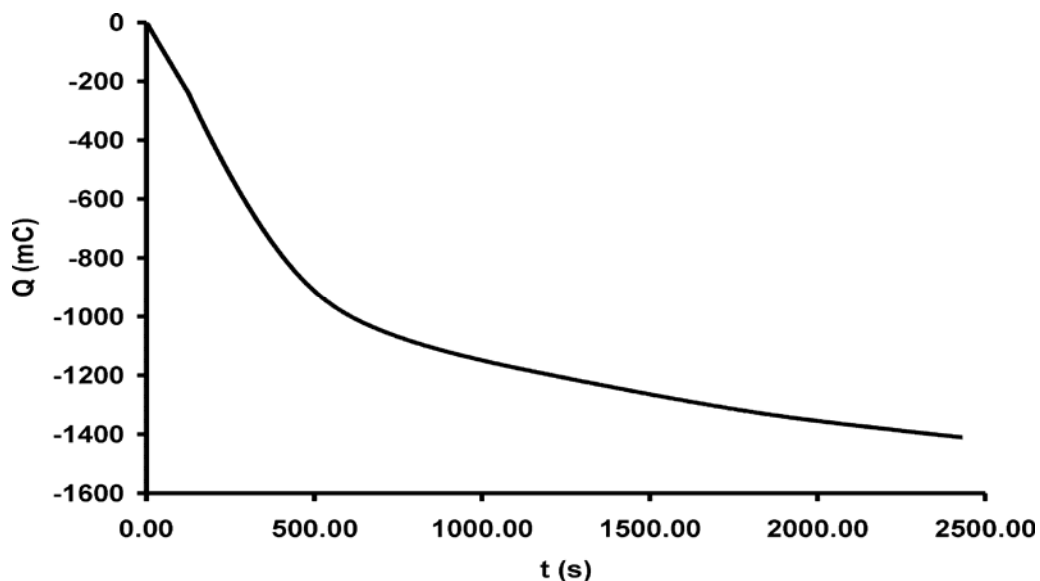


Figure III-2. Plot of charge versus time acquired during oxidation of **1a** to **1b** at -20 °C.

Prior to initiation of the oxidation, the UV-visible spectrum of **1a** was recorded. During the oxidation of **1a** to **1b**, the UV-visible spectrum of the solution was monitored, Figure III-3. The UV-visible spectrum of **1a** in acetonitrile shows a weak absorption band at 435 nm. During oxidation, the color of the solution changed from yellow to brown. New absorption bands at 540 nm, 797 nm, and 1041 nm were observed. Spectra were recorded approximately for every one tenth of the electron equivalent during oxidation of **1a** to **1b**.

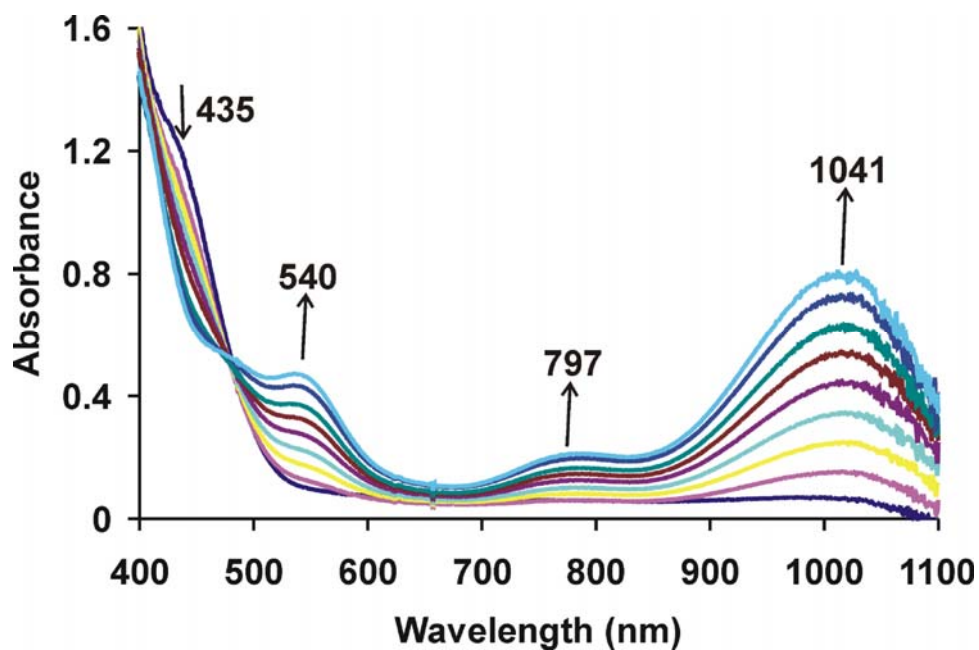


Figure III-3. Electronic spectra obtained during oxidation of **1a** to **1b**. Spectra were obtained approximately for every one tenth of electron equivalent in MeCN solution at $-20\text{ }^{\circ}\text{C}$.

To the freshly prepared solution of **1b**, ethylene gas was purged continuously through the solution during the following oxidation. Complex **2b** was generated by the bulk oxidation of **1b** at a potential of $+620\text{ mV}$. The oxidation was stopped when the current returned to background levels. A coulometric charge of 1049 mC corresponding to 0.83 electron equivalent was obtained.

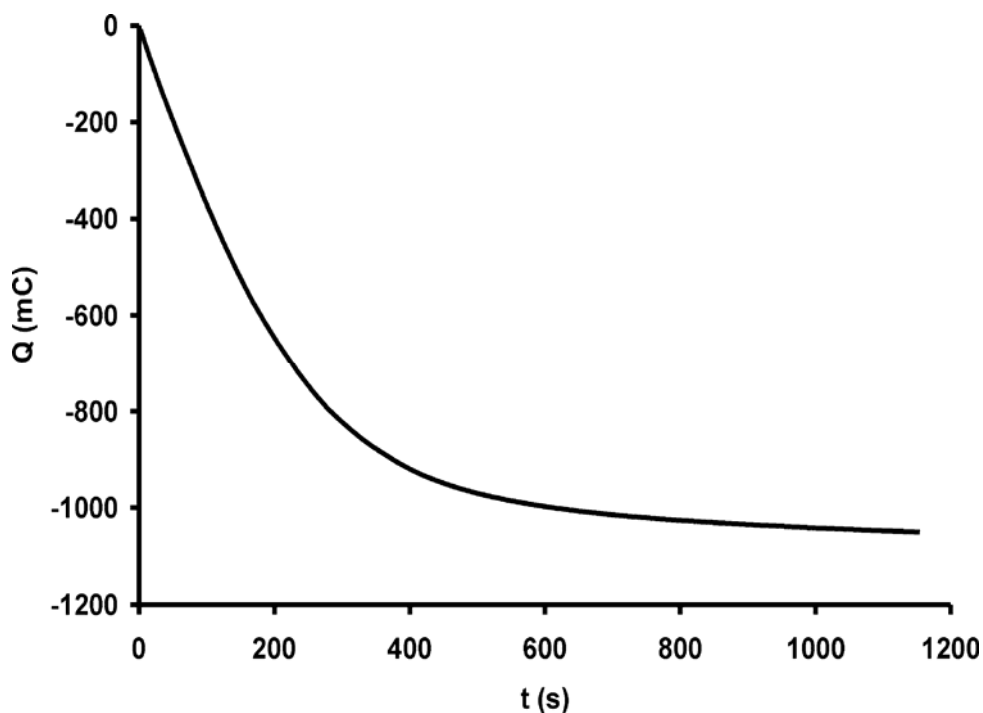


Figure III-4. Plot of charge versus time acquired during oxidation of **1b** to **2a** at $-20\text{ }^{\circ}\text{C}$.

During the oxidation of **1b** in the presence of ethylene, the UV-visible spectrum of the reaction mixture was monitored. Spectra were recorded approximately every one tenth of the electron equivalent during oxidation of **1b**, Figure III-5. During the oxidation, there was continuous decrease in intensity of absorption bands at 540 nm, 797 nm and 1041 nm and the color of the solution has been changed to yellow. Upon the completion of the oxidation, the electronic spectrum was silent between 400 nm to 1000 nm. The UV-visible trace also does not display any intermediates or isosbestic points. The intermediate at 850 nm which is generally observed during oxidation of **1b** is not seen in the presence of ethylene. This is consistent with the rapid reaction of the radical intermediate with ethylene.

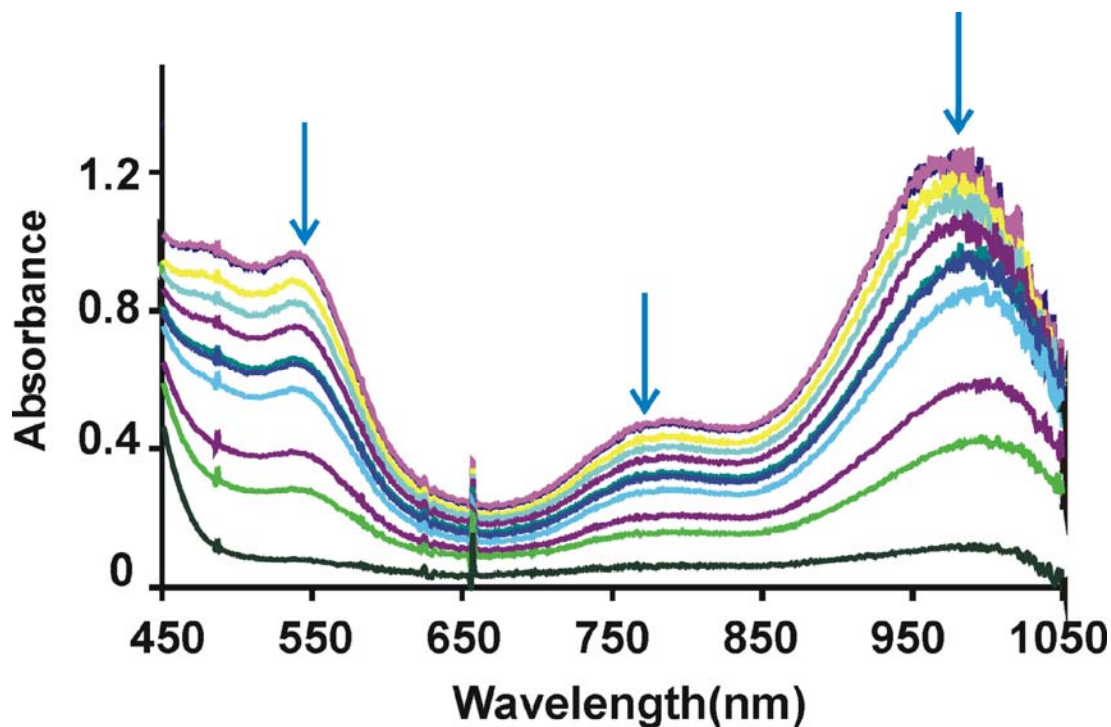


Figure III-5. Electronic spectra obtained during oxidation of **1b** to **2a**. Spectra were obtained approximately for every one tenth of electron equivalent in MeCN solution at -20 °C.

The square wave voltammogram recorded after this oxidation, Figure III-6, reveals a significant change in the coordination environment of the ruthenium. The voltammogram reveals a single event at around +800 mV. This potential is similar to that observed for the disulfide product obtained in acetonitrile and the methylene bridged compound reported previously.^{19,21} This is not unexpected as all the complexes have a similar coordination environment. To further understand the differences between **2a** and the disulfide complex generated in acetonitrile, stability tests were conducted. Solution samples of each were generated electrochemically at -20 °C. Each sample was then allowed to warm to room temperature and stand open to air for 24 hours. A square wave

voltammogram of **2a** showed no detectable change, while the square wave voltammogram of the disulfide showed a loss of intensity at +800 mV and the appearance of various smaller signals. This clearly shows that **2a** is a unique product and not the disulfide complex.

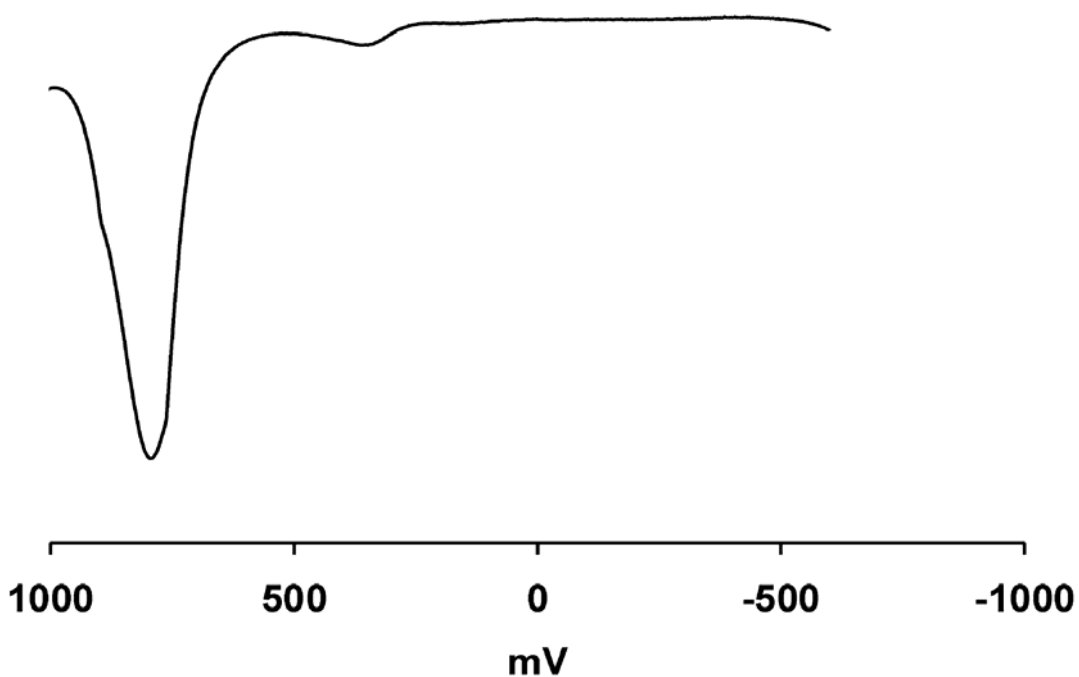


Figure III-6. Square wave voltammogram of **2a** in acetonitrile with 0.1 M TBAHFP at -20°C . Potentials referenced to Ag/AgCl.

As mentioned previously, the square wave voltammogram of **2a** displays a single redox event at +804 mV. This event is assigned as a Ru(III)/(II) couple, which is shifted by +1151 mV as compared to the trithiolate, **1a**, Figure III-7. Earlier reports by the Darensbourg group indicate a shift of this value is consistent with the conversion of two

anionic thiolate donors to neutral thioethers.²⁵ Importantly, no reduction events are observed even though the product is two electrons more oxidized than **1a**.

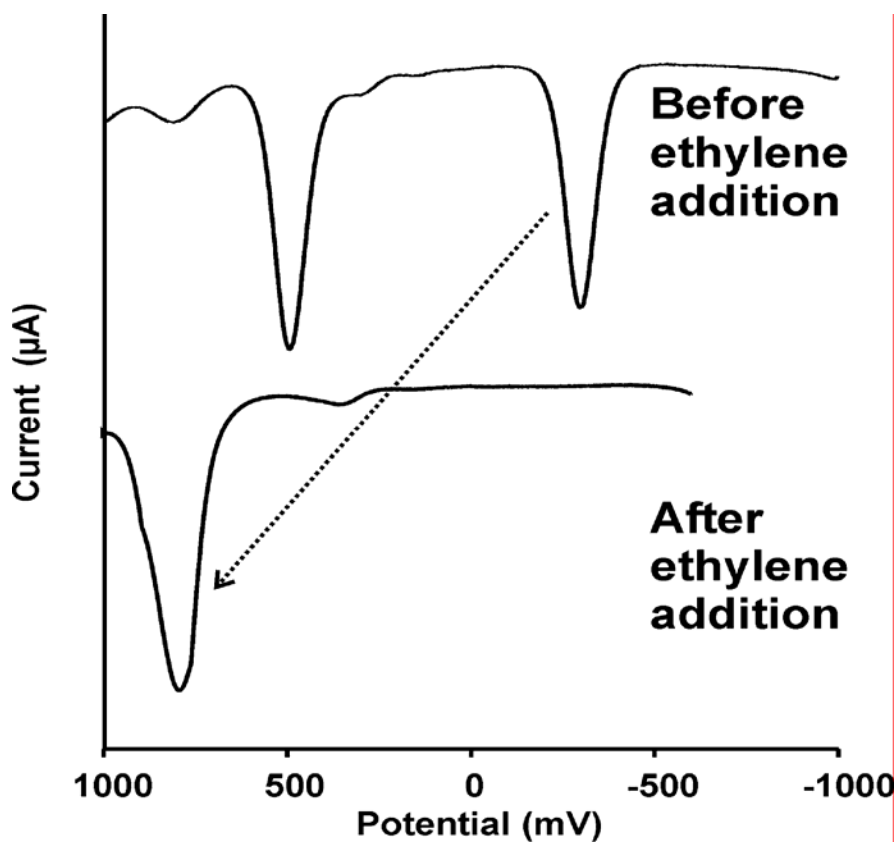
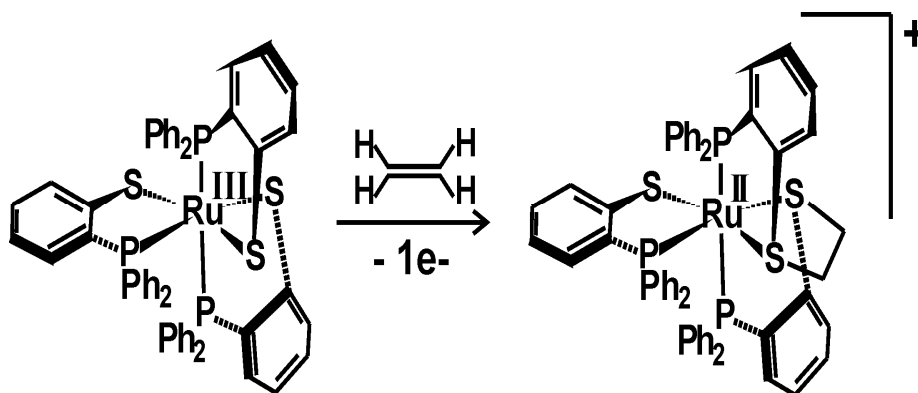


Figure III-7. Comparison of square wave voltammogram of **1b** and **2a**.

From the electrochemical investigations and electronic spectroscopy it can be clearly understood that there is formation of a Ru(II)-dithioether product, **2a**, Scheme III-7. This is proposed to result via an EC mechanism in which **1b** is oxidized to **1c** in the electrode step and then **1c** reacts with ethylene to form **2a** in the chemical step.

Scheme III-7.



As mentioned previously, **2a** displays a single redox event at +804 mV. This represents a further oxidation that is assigned as a Ru(III)/Ru(II) couple. To confirm this assignment, the light yellow color product **2a** was oxidized to **2b** at a holding potential of +1000 mV. Again, the potential was applied until the current decayed to less than 5% of the initial value. The oxidation was complete after ~1200 seconds and the total charge produced was 1326 mC, Figure III-8. This represents 1.05 electron equivalents. The charge produced in this reaction confirms the oxidation is a one electron event per ruthenium. The square wave voltammogram was taken following oxidation and it again showed a single event ~804 mV. This indicates there is no change in the ligand donor environment during oxidation of **2a** to **2b**.

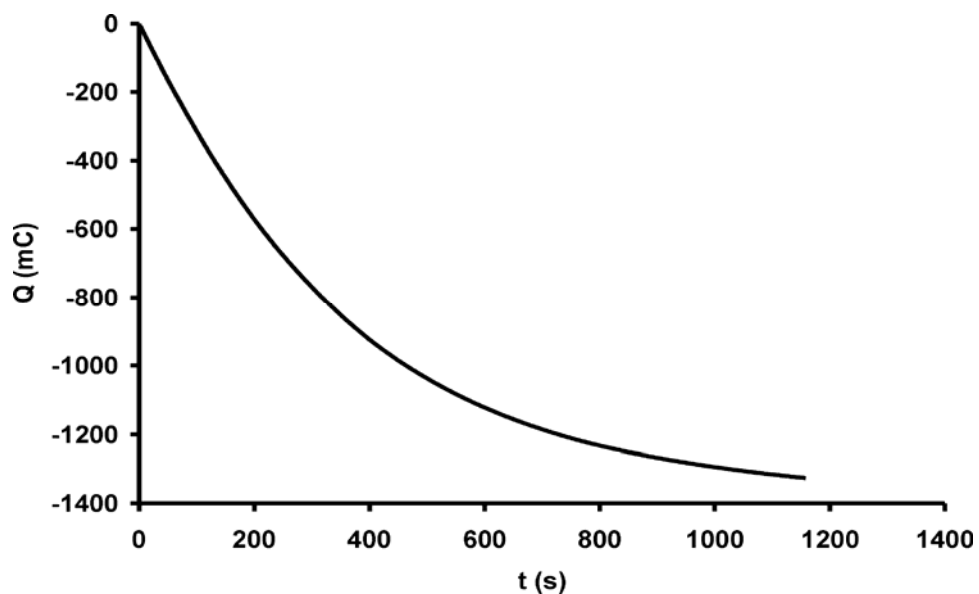


Figure III-8. Plot of charge versus time acquired during oxidation of **2a** to **2b** at $-20\text{ }^{\circ}\text{C}$.

The bulk oxidation of **2a** to **2b** was monitored *in situ* by UV-visible spectroscopy. The color of the solution changed from yellow to green. As shown in Figure III-9, there is a continuous increase in the intensity of an absorption band at 690 nm during the oxidation, which can be assigned as a thiolate to metal charge transfer band consistent with a Ru(III) oxidation state.¹⁹ From the solution of **2b**, an aliquot was taken by microliter syringe and frozen at 77 K for EPR analysis (*vide infra*). Finally a holding potential of +700 mV was applied to reduce **2b** back to **2a**. During the bulk electrolysis there was continuous decrease in the intensity of the signal at 690 nm and the solution turned to yellow in color. Once bulk electrolysis was completed, the electronic spectrum was silent between 400 to 1000 nm, indicating formation of **2a**.

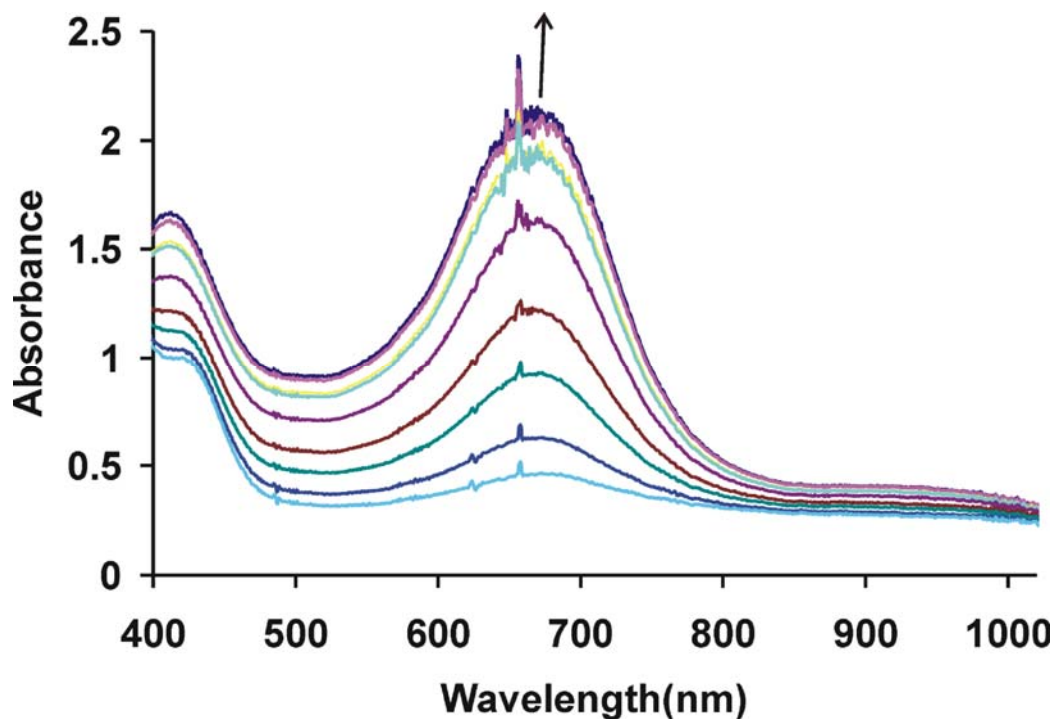


Figure III-9. Electronic spectra obtained during oxidation of **2a** to **2b**. Spectra were obtained approximately for every one tenth of electron equivalent in MeCN solution at $-20\text{ }^{\circ}\text{C}$.

Characterization

To further enhance knowledge of **2a**, + ESI-MS was employed. The crude sample of **2a** was obtained by removing all solvent under vacuum. This method yields a residue that is primarily comprised of supporting electrolyte (TBAHFP), but with small quantities of **2a**. The parent ion peak for **2a** was found at $m/z = 1009.1013$ amu, which is within experimental error of the theoretical value of 1009.1018 amu.³⁰ The isotopic envelope of the parent ion of **2a** shows a similar pattern to that of the theoretical one, Figure III-10. From these observations, it is quite evident that the reaction between **1a** and ethylene to form **2a** was successful.

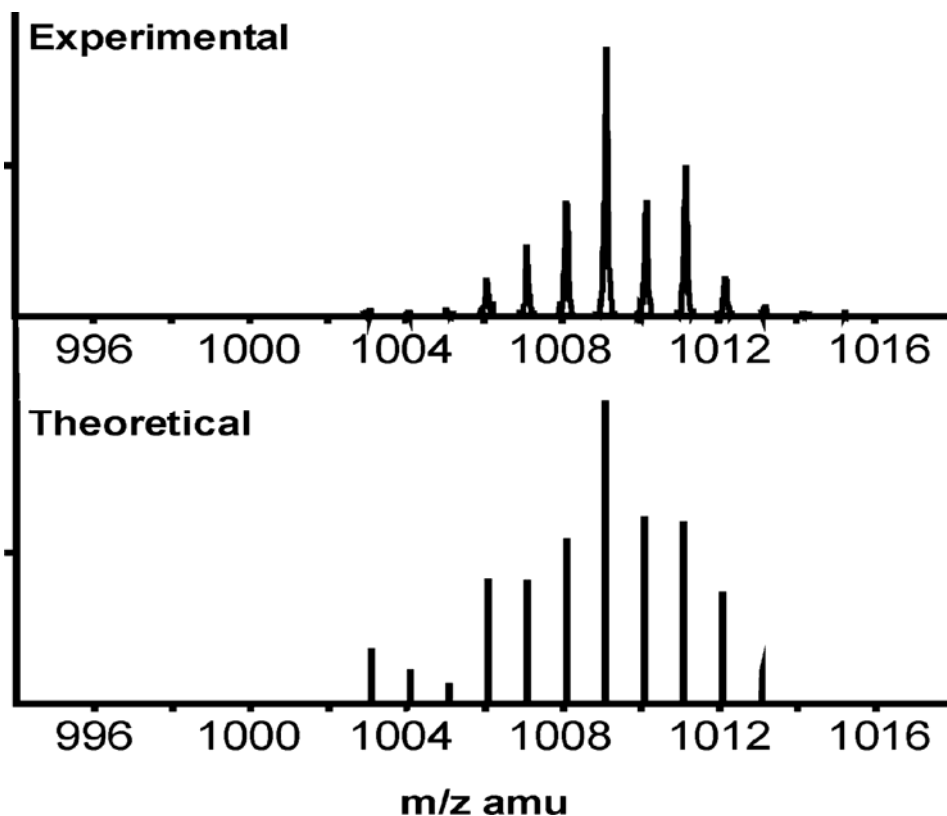


Figure III-10. +ESI-MS of **2a** in acetonitrile.

The phosphorus environment about ruthenium in **2a** was probed by ^{31}P NMR. The samples of **2a** for NMR spectroscopy were prepared by drying the compound under vacuum and then dissolving the same in a small amount of deuterated acetonitrile. Finally the samples were filtered through fritted septa of 13 mm syringe filter with 0.2 μm PTFE membrane into a NMR tube. The experimental NMR spectra were simulated using the Frequnt program to determine chemical shift values and coupling constants.³¹ The ^{31}P NMR spectrum of **2a** shows three chemical shifts at 61.0 ppm, 40.3 ppm and 37.5 ppm, Figure III-11. There is one large coupling constant with a value of 304 Hz and two smaller values estimated to be 30 Hz each. These coupling constant values indicate the 3

phosphorus donors are arranged in a meridional fashion about the Ru(II) ion.^{21,32} The larger coupling constant occurs between trans phosphorus donors, and the smaller coupling occurs between cis phosphorus donors.³³ Chemical shift values and coupling constant values are close to the expected values of phosphorus in **1a**. From this data it is quite evident that there has been no change around the phosphorus environment.

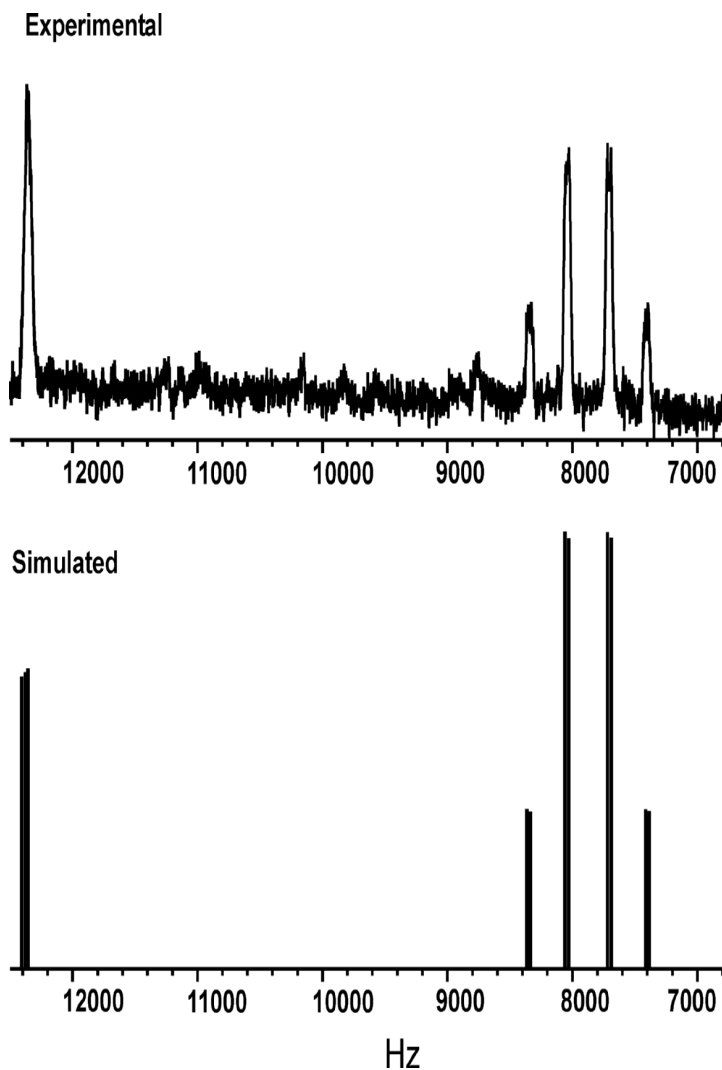


Figure III-11. ³¹P NMR spectrum of **2a** in deuterated acetonitrile. ³¹P NMR spectrum was simulated by using Freqint program.

EPR analysis of the frozen aliquot of **2b** was done at 77 K in an EPR Suprasil quartz dewar. The microwave frequency was set to 9.6011 GHz and the power held at 1.978 mW. The experimental data was simulated by using SIMPOW to extract g values.³⁴ The EPR of **2b** displays a rhombic signal with $g_1 = 2.09$, $g_2 = 2.03$, $g_3 = 2.04$, Figure III-12. This is consistent with an $S = \frac{1}{2}$ system with ruthenium in the +3 oxidation state. However the g-values cannot be explained by simple rotational relationships and spin orbit coupling.³⁵ Additionally attempts to model the g-values using the approach of Taylor developed for a d^5 low-spin heme iron does not yield physically reasonable conclusions.³⁶ This complexity is attributed to the high covalency of the Ru-S bond which makes assignment of the oxidation state difficult. The observed g values are similar to the values reported by Wieghardt for metal coordinated thiyl radicals.¹³ Therefore, the EPR of **2b** is consistent with a product that contains Ru(III) thioether and Ru(II) thiyl radical character.

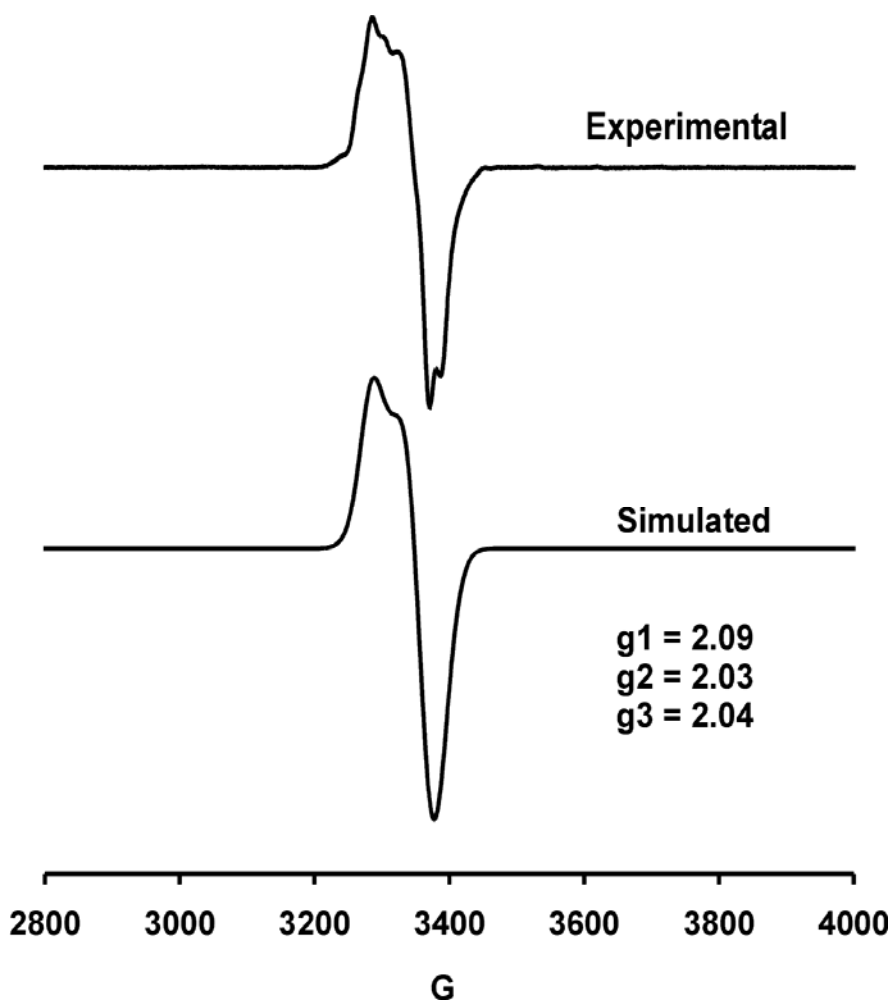


Figure III-12. EPR spectrum of **2b** at 77k. Experimental Conditions: microwave frequency of 9.6011 GHz; microwave power 1.978 mW, modulation frequency 100 kHz, modulation amplitude of 10 G. Line widths for simulated spectrum : $W_x = 32$, $W_y = 39$, $W_z = 37$.

Reactivity of **1c** with various other alkenes

As noted above, the intermediate **1c** was generated in the presence of various other alkenes. Spectroscopic results are highlighted in Table III-1. Figures for the same

have been provided in the appendix. The experimental protocol is the same as described for ethylene with the following exception. A single portion of the alkene as a liquid or solid was added to the solution prior to the oxidation of **1b** to **1c**.

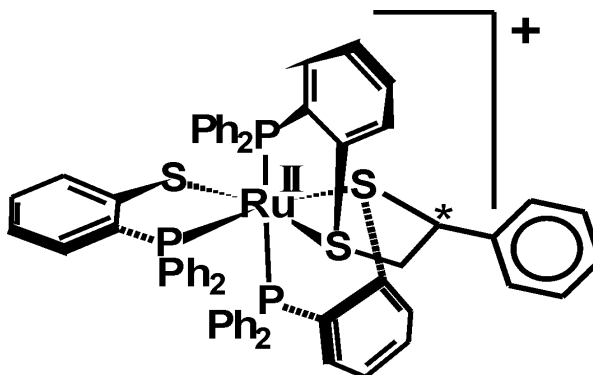
The +ESI-MS spectra of **3a**, **4a**, **5a**, and **6a** show the expected parent ion peaks with the predicted isotopic pattern. The accuracy of the experimental m/z ratio with respect to the theoretical value is ~ 1 ppm. These data indicate the successful addition of each tested alkene to **1c** to yield the respective products.

The ^{31}P NMR spectra of **3a**, **4a**, **5a**, and **6a** show coupling constants and chemical shift values that are very close to that of anticipated values and are very much similar to the data acquired from **2a** indicating that the phosphorus environment has not changed. The ^{31}P NMR spectrum of **4a** is unique as it shows two sets of peaks consistent with two similar, but non-magnetically equivalent meridional P_3 donor sets. This is attributed to the presence of 2 isomers of **4a**, which contains a new chiral carbon atom as shown in Scheme, III-8.

The $E_{1/2}$ potentials for the $\text{Ru}^{\text{III/II}}$ couples of **3a**, **4a**, **5a**, **6a**, Table III-1, indicate that they are very close to each other and also to that of **2a** (within experimental error). The $E_{1/2}$ values range from +792 mV to +824 mV, consistent with a shift of around +1100 mV from **1a** indicating alkylation of 2 anionic thiolates to form dithioethers.²⁵

Table III-1. Square wave voltammogram, +ESI-MS, and ^{31}P NMR of 3a , 4a , 5a , and 6a				
Spectroscopic method	3a	4a	5a	6a
ESI-MS (amu)	1065.1655	1085.1317	1063.1493	1075.1478
^{31}P NMR				
Coupling constant (Hz)	30, 30, 318	30, 30, 300 (I) 30, 30, 311(II)	30, 30 313	30, 30, 315.
Chemical shift (ppm)	59.0, 40.0, 38.8	56.3, 45.9, 37.5 (I) 61.0, 40.7, 36.6 (II)	56.2, 41.1, 38.1	57.3, 40.0, 37.0
Electrochemistry				
$E_{1/2}$ (mV)	+792	+788	+790	+824

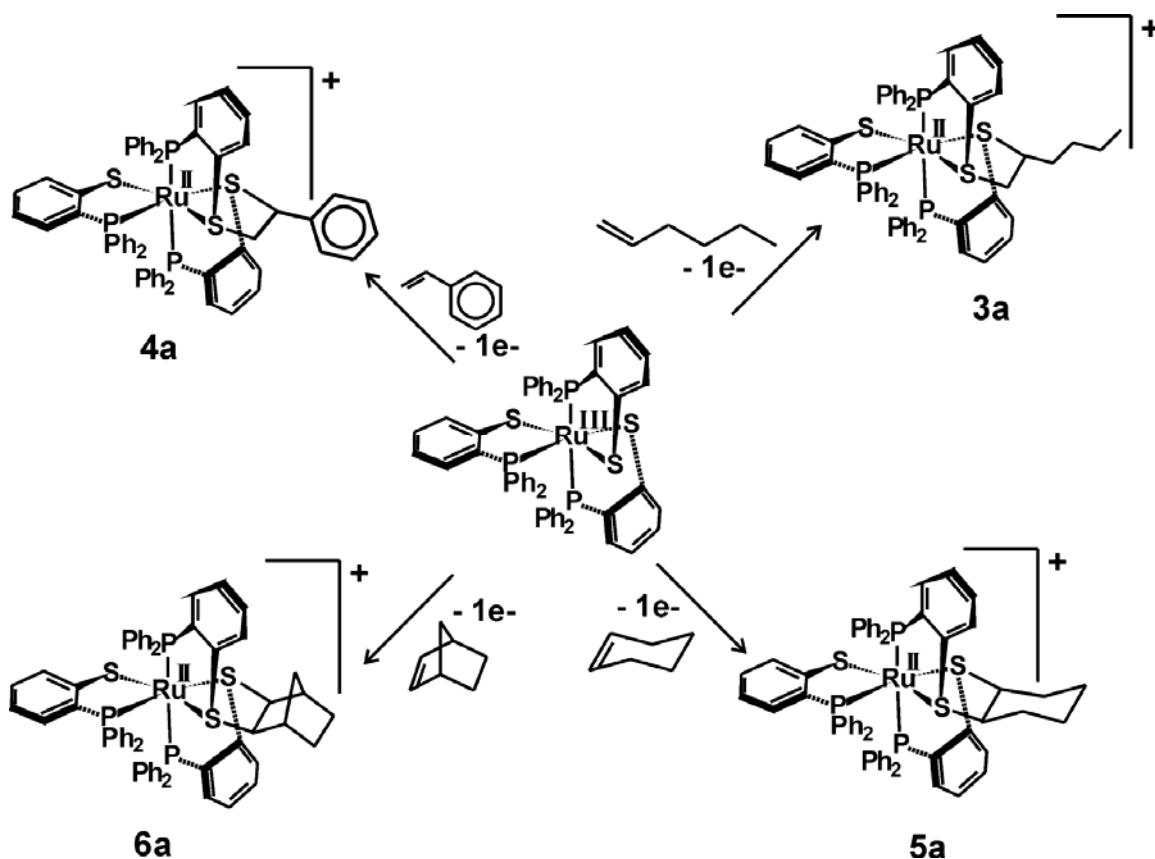
Scheme III-8.



All the above mentioned data from various spectroscopic techniques clearly indicate that **1c** reacts with various alkenes to yield respective Ru(II) dithioether compounds, Scheme III-9. The spectroscopic data obtained give similar results to the

extensively described reaction of **1c** with ethylene.

Scheme III-9.



Just as **2a** can be oxidized to **2b**, the corresponding Ru(II)-dithioether complexes were oxidized to **3b**, **4b**, **5b**, and **6b**. Spectroscopic results are tabulated in Table III-2. Each complex has a single absorbance band in the visible region with λ_{\max} values for **3b**, **4b**, and **5b** in the range of 682 nm to 697 nm. These bands are assigned as charge transfer bands from the thiolate to the metal. The λ_{\max} value of **6b** was not determined owing to solubility problems.

The EPR data of **3b**, **4b**, **5b**, and **6b** are very similar to each other and also to **2b**

with rhombic signals. The three different g-values range from 2.02 to 2.09. The g-values of **3b**, **4b**, **5b**, and **6b** confirm ruthenium is in the formal +3 oxidation state and it constitutes to $s = \frac{1}{2}$ system.

Table2. Electronic absorption maximum and EPR g-values of **3b**, **4b**, **5b**, and **6b**

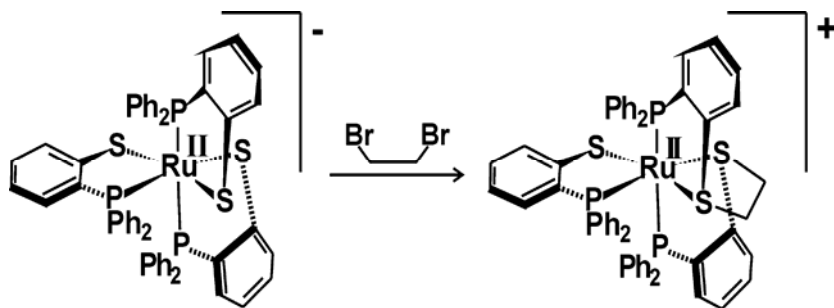
Spectroscopic method	3b	4b	5b	6b
Electronic Spectrum				
λ_{max} (nm)	682	692	697	N.A.
EPR				
g_1	2.08	2.09	2.09	2.09
g_2	2.03	2.05	2.05	2.05
g_3	2.02	2.03	2.02	2.03

While X-ray crystallography provides the most definitive assignment of structure, single crystals could not be obtained from the electrochemically generated products. This is attributed to the small quantity of product generated and the presence of large amounts of the supporting electrolyte. Hence, an independent chemical synthesis of **2a** was undertaken to confirm the structure.

Chemical Synthesis

In the electrochemical synthesis, the oxidized complex **1c** adds ethylene to generate the observed product **2a**. In the chemical synthesis of **2a**, 1,2-dibromoethane was reacted with **1a**, to yield **2a**, Scheme III-10. When the ethylene bridge is generated from dibromoethane, which is two electrons more oxidized than ethylene, complex **1a**, which is two electrons more reduced than **1c**, is the appropriate ruthenium source.

Scheme III-10.



The complex **2a** was prepared by adding 7.4 μL of 1,2-dibromoethane to a chlorobenzene solution of **1a** in a 50 mL Schlenk flask. The reaction mixture was stirred overnight resulting in a dark brown solution. This dark solution was filtered through Celite to remove PPNCl . The resulting filtrate solution was then transferred via syringe through a 13 mm syringe filter with 0.2 μm PTFE membrane into a small test tube. The resulting brown solution was further layered with a small amount of the diethyl ether. After 2 days, yellow colored crystals of **2a** were obtained.

Spectroscopically, the **2a** products from the chemical method and from the electrochemical method are identical. This was confirmed by all applicable techniques including electrochemistry, mass spectrometry, and ^{31}P NMR as tabulated in Table III-3. The square wave voltammogram from the two methods show $E_{1/2}$ values of +794 mV and +804 mV, which is within experimental error. The mass spectra show parent peaks at 1019.1013 amu and 1019.1015 amu. Furthermore the ^{31}P NMR of both the products show very similar spectra with nearly identical values for coupling constants and chemical shifts. From the above data, it can be inferred that chemically synthesized and electrochemically generated products are indistinguishable from each other.

Table III-3. Comparison of square wave voltammogram, +ESI-MS, and ³¹P NMR of chemically and electrochemically generated **2a**

Spectroscopic method	2a (chemically generated)	2a (electrochemically generated)
ESI-MS (amu)	1009.1015	1009.1013
³¹P NMR		
Chemical shift (ppm)	61.8, 40.7 and 37.7	61.0, 40.3 and 37.5
coupling constant (Hz)	30, 30, and 312	30, 30 and 304
Electrochemistry		
E _{1/2} (mV)	+794	+804

Yellow X-ray quality crystals of **2a** were obtained by layering diethyl ether directly onto the filtered chlorobenzene reaction solution containing crude product. Single crystal selection, collection of x-ray diffraction data, and the solving and refinement of the data were performed by Dr. Mark Mashuta at the X-ray Diffraction Laboratory at the University of Louisville Department of Chemistry.³⁷⁻⁴² Compound **2a** crystallizes in the monoclinic space group P2₁/c with unit cell dimensions of a = 10.2565(9) Å, b = 13.2338(12) Å, c = 38.325(3) Å, and β= 93.3960(10)°. An ORTEP representation of the ruthenium containing cation of the asymmetric unit is shown in Figure III-13. The bromide counter ion is not shown. Additionally, the crystal contains one chlorobenzene molecule per asymmetric unit.

The cation of **2a** contains a single ruthenium ion situated in a pseudo-octahedral P₃S₃ donor environment. Two of the sulfur donors, S2 and S3, are thioether donors resulting from the alkylation of the trithiolate precursor, **1a**. The P(3)-Ru-P(2) bond angle is 168.81(3)°. The P(1)-Ru-P(3) bond angle is 93.62(3)°, which is slightly smaller than

the similar bond angle in **1a**.²¹ In both cases, the P-Ru-P moved towards ideal bond angles of 180° and 90°. All of the bond angles involving the thioether sulfurs show some interesting facts. The P(1)-Ru(1)-S(2) bond angle is 172.87(3)° while the S(3)-Ru-P(3) bond angle is 85.55(3)°. These are very close to the corresponding bond angles in **1a**. This indicates there is no significant strain imposed by formation of the thioether bridge. The S(3)-Ru(1)-S(2) bond angle of 87.71(3)° is also close to the corresponding angle in **1a** consistent with the lack of additional strain.²¹

The Ru-P distances range from 2.3290(9) Å to 2.3965(10) Å and these values are slightly greater compared to previously reported Ru-P values for [Ru(DPBTT)₂CH₂](DPPBT)]Cl.²¹ In [Ru(DPBTT)₂CH₂](DPPBT)]Cl, which also contains cis thiolates that have been alkylated, there is formation of a methylene bridged thioether.²¹ The Ru-S(1) bond length is 2.3856(9) Å and is close to previously reported Ru-S_{thiolate} bonds.⁴³⁻⁴⁶ The Ru-S thioether bond lengths in **2a** for Ru-S2 and Ru-S3 are 2.3749(9) Å and 2.3365(9) Å respectively. These values are slightly shorter than the previously reported values of Ru-S(2) and Ru-S(3) of 2.406(1) Å and 2.358(1) Å in [Ru(DPBTT)₂CH₂](DPPBT)]Cl.²¹ This decrease in bond length can be attributed to release of geometrical constraint due to formation of a 5 membered ring as opposed to a 4 membered ring in the methylene bridged thioether. The carbon sulfur bond lengths for S(2)-C(55) and S(3)-C(56) are 1.836(4) Å and 1.843(4) Å, respectively. These values are very close to expected values for a C-S single bond.⁸

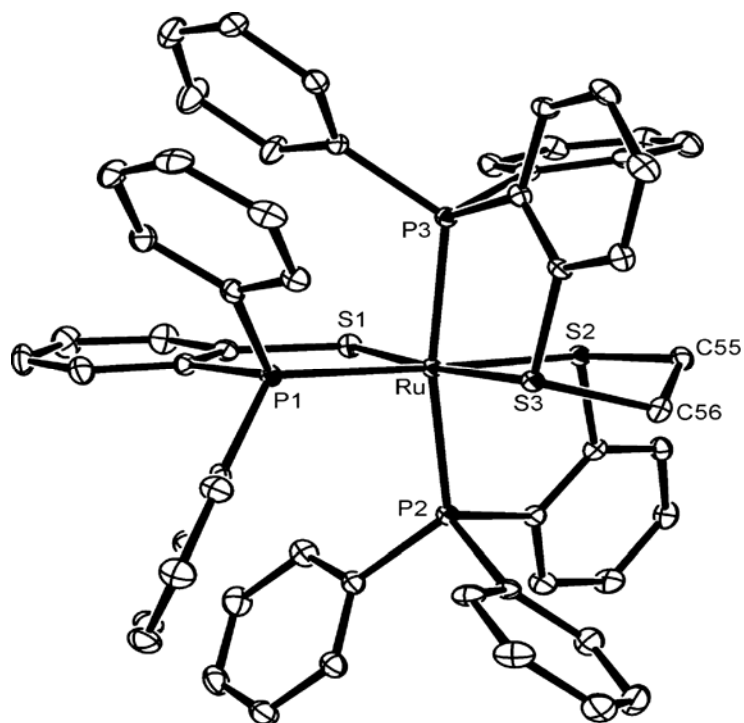


Figure III-13: An ORTEP⁴⁷ diagram of the cation of **2a** with partial atom labeling scheme. Important bond lengths [Å] and angles [°]: Ru-P(1) 2.3290(9), Ru-P(2) 2.3965(10), Ru-P(3) 2.3648(9), Ru-S(1) 2.3856(9), Ru-S(2) 2.3749(9), Ru-S(3) 2.3365(9), S(2)-C(55) 1.836(4), S(3)-C(56) 1.843(4), C(55)-S(2)-Ru 104.52(12), C(56)-S(3)-Ru 103.59(12), C(55)-C(56)-S(2) 114.0(3), C(55)-C(56)-S(3) 112.8(3)

Mechanistic insight

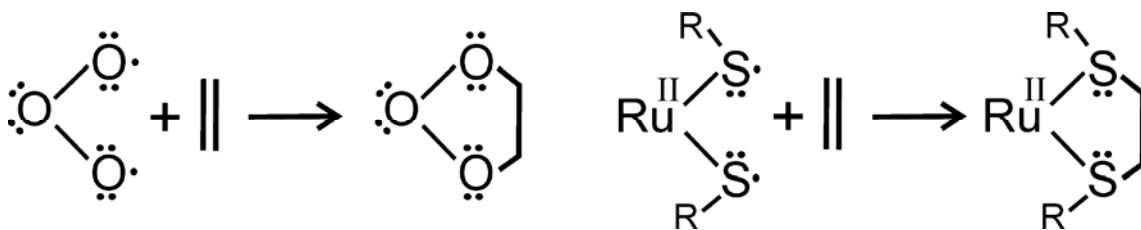
The following important conclusions can be made from this study. The oxidized intermediate complex **1c** reacts with different alkenes to form two new carbon-sulfur bonds. The formation of these C-S bonds yields a dithioether which contains cis sulfur donors linked by carbon atoms provided by the alkene. The net result is the Ru-S core of **1a** is reduced by two electrons while the alkene undergoes a two electron oxidation.

The reactivity of **1c** with alkenes is comparable to its reactivity with the enol

tautomer of methyl ketones reported previously.²⁰ A key difference is the observation of the absorbance band of **1c** at 850 nm in the electronic spectrum during reaction with the latter, but not the former. This is attributable to the relatively small enol concentration in methyl ketone solutions that permits **1c** to accumulate. In the alkene reactions, sufficient alkene concentrations are maintained for the reaction with **1c** as rapidly as it is generated.

A proposed mechanism for the reaction of **1c** with alkenes was developed with the help of recent DFT studies by the Grapperhaus group.⁴⁸ The DFT work will be the focus of Holly Frye's Thesis. Based on the DFT studies, **1c** is best described as having a singlet diradical ground state. This singlet diradical ground state can be represented with contributions described as a Ru(II)-dithiyl radical, which is isoelectronic with the ground state of ozone.⁴⁹ As such, the reactivity of **1c** towards alkenes may be very much similar to the reactivity of ozone towards alkenes. When ozone reacts with an alkene, the initially formed product is an ozonide.⁴⁹ In a similar fashion, **1c** reacts with alkene to form a Ru(II) dithioether, Scheme III-11. Whether this reaction is concerted or stepwise is not completely understood.

Scheme III-11.



CHAPTER IV

CONCLUSIONS

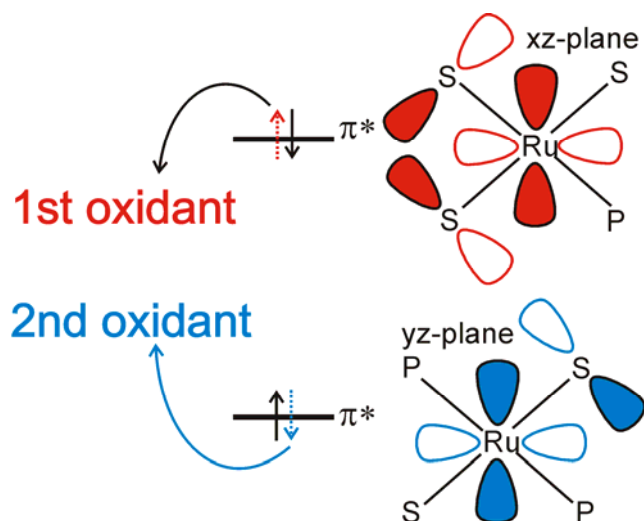
As highlighted in Chapter III, the oxidation of the ruthenium trithiolate complex, $[\text{Ru}(\text{DPPBT})_3]^-$, proceeds in two one-electron steps. The first oxidation, previously assigned as metal-centered, can be readily accomplished by applying a potential of +100 mV. The product, $[\text{Ru}(\text{DPPBT})_3]$, can be further oxidized to $[\text{Ru}(\text{DPPBT})_3]^+$ by holding the applied potential at +620 mV. The fully oxidized complex, $[\text{Ru}(\text{DPPBT})_3]^+$, displays sulfur based reactivity leading to C-S bond formation. This has been attributed to a sulfur-centered oxidation yielding a reactive metal-coordinated thiyl radical.

The sulfur based reactivity was previously attributed to formation of a reactive metal-coordinated thiyl radical. The proposed thiyl radical displays an absorption band in the visible region at 850 nm in acetonitrile when generated at low temperature. However, the radical decays to a disulfide complex that is also thermally unstable. Also in acetone or other methyl ketones, the radical intermediate is observed. In these solvents, decay of the radical results in C-S bond formation and isolation of a thioether product.

Recent density functional theory (DFT) investigations by Holly Frye in the Grapperhaus group in a collaborative project with Professor Pawel Kozlowski have sought to determine the ground state of the reactive intermediate, $[\text{Ru}(\text{DPPBT})_3]^+$.⁴⁸ Full details of this work will be presented in Mrs. Frye's thesis. From her studies, the ground state of $[\text{Ru}(\text{DPPBT})_3]^+$ is best explained as singlet diradical.

As shown in Scheme IV-1, the diradical ground state results from subsequent oxidations of nearly degenerate M-S π^* orbital's. This diradical has unpaired electrons delocalized over the metal and sulfur donors in nearly orthogonal orbitals. The relative orientation of the half occupied orbital inhibits disulfide formation as a large structural rearrangement is required for S-S bond formation. However, the orbital arrangement favors addition of unsaturated hydrocarbons across the cis-sulfur atoms.

Scheme IV-1.



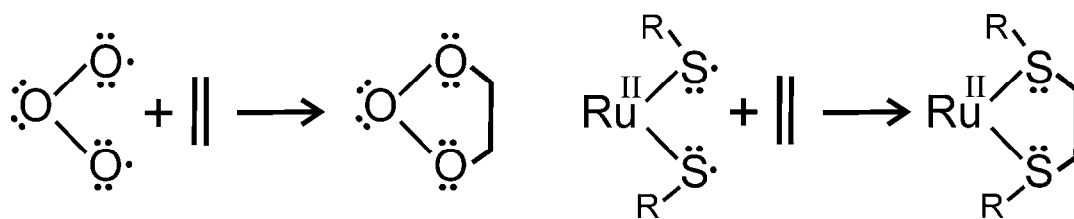
The addition of alkenes to $[\text{Ru}(\text{DPPBT})_3]^+$ occurs so rapidly that the signature band at 850 nm is not observed when bulk oxidation at +620 mV is performed in the presence of alkenes. The 850 nm band is observed in the presence of ketones. It is hypothesized that this is because only the enol tautomer is reactive and the concentration of the enol is low. In fact, when the enol tautomer was stabilized, reactivity was observed with no detectable intermediate.

The diradical generated can react with various alkenes at rates sufficient to prevent observation of the intermediate. This efficiency of reactivity was proven by reactions with alkenes ranging from simple alkenes, like ethylene, to bulkier, bridged alkenes, like norbornene. In all cases, the observed product is a Ru(II)-dithioether.

The diradical ground state of $[\text{Ru}(\text{DPPBT})_3]^+$ can be compared to the generally accepted ground state of ozone. Ozone and the $[\text{Ru}(\text{DPPBT})_3]^+$ are isoelectronic, with both of them having total of 18 valence electrons. Apart from being isoelectronic both of them are diradical species, (in case of ozone terminal oxygen's function as diradicals and in case of $\text{Ru}(\text{DPPBT})_3^+$, cis sulfurs act as diradicals).

Ozone reacts with alkenes to generate, initially, a primary ozonide in either stepwise or concerted mechanism; in a similar fashion $[\text{Ru}(\text{DPPBT})_3]^+$ diradical reacts with alkenes to form the dithioether product, Scheme IV-2. This results in formation of two C-S bonds and a bridge between cis sulfur donors.

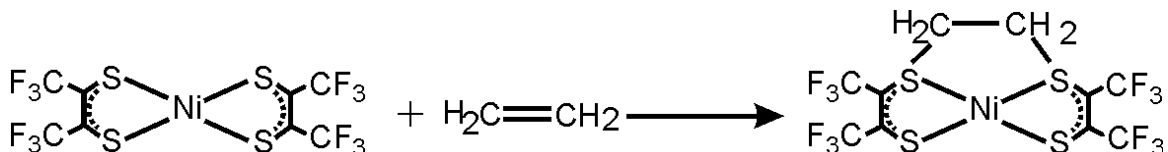
Scheme IV-2.



The cis arrangement of sulfur donors facilitates alkene adduct formation in an inter-ligand fashion. This type of interaction was earlier reported by Stiefel and coworkers upon oxidation of nickel dithiolenes, Scheme IV-3. In the experiments conducted by Stiefel group, nickel dithiolenes oxidized to promote alkene addition and

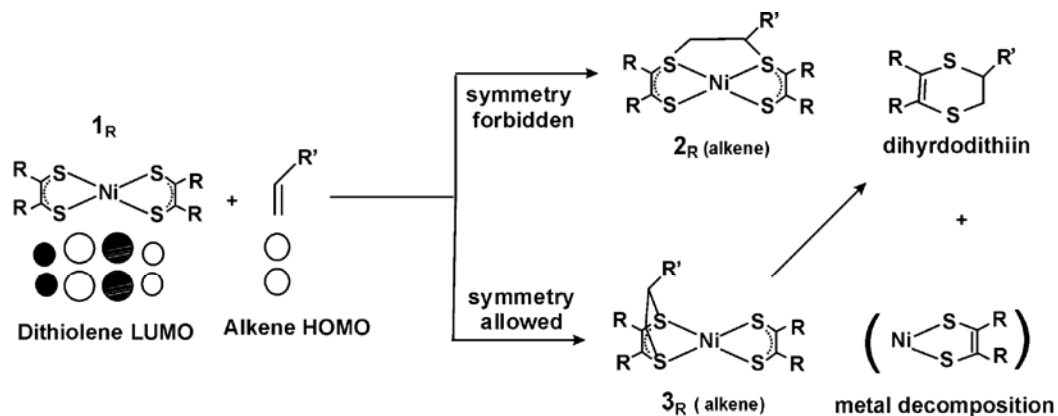
then reduced to facilitate alkene dissociation.²⁸ This intriguing result offered promise for the use of nickel dithiolenes for redox controlled reversible olefin binding as a means for olefin purification.

Scheme IV-3.



However, recent studies by Fekl and coworkers indicates that the above mentioned reaction favors the addition of an alkene to nickel dithiolenes in an intra-ligand fashion, as opposed to the inter-ligand addition mechanism which was predicted by the Stiefel group, Scheme IV-4. The intra-ligand alkene adduct that is formed, further decomposes into dihydrodithiin and metal-decomposition products.²⁹

Scheme IV-4.



In the case of $[\text{Ru}(\text{DPPBT})_3]^+$, the addition of alkenes is undoubtedly intra-ligand. The resulting dithioether product is thermally stable. In addition, the product is air, light, and water stable. As such, $[\text{Ru}(\text{DPPBT})_3]^+$ has several advantages over nickel dithiolenes for olefin purification.

Past investigations by the Rothlisberger group revealed that Ru(II)-thioethers cannot undergo C-S bond cleavage, making the alkene addition reaction irreversible, and liberation of the alkenes impossible under the current reaction conditions.⁵⁰ The liberation require reduction to Ru(I) ($t_2g^6 e_g^1$), which is not feasible. The purposed pathway for the cleavage of C-S bonds indicates that ruthenium as the metal center cannot be useful for alkene liberation reactions. It can still be useful in reactions with methacrylate and methyl methacrylate which are environmental toxins and are assumed to react with sulfur centered radicals. This reactivity will be further investigated.

In our future directions the reactivity of the radicals with alkenes with electron withdrawing groups like acrylonitrile and cis-dichloroethane will be done to understand the reactivity of sulfur centered radical, as they are known to react slowly with them.

Another important reaction will be done to see whether the diradical will react more preferentially towards a thiol group to form a disulfide or will react with unsaturated double bond. To prove this, a compound which has both double bond and a thiol group will be taken and will be reacted with singlet diradical. This comparison of reactivity can lead to many interesting facts.

The importance of the metal in reversibility of the reaction will also be further studied in Grapperhaus group.⁵¹ If rhenium is used instead of ruthenium then reversibility of the reaction can be easily done as Re(II) (t_2g^5) to Re(I) (t_2g^6) reduction is

thermodynamically favorable and C-S bond cleavage can be expected. This will make the whole reaction of removing olefin or other unsaturated compounds more feasible.

REFERENCES

1. <http://goldbook.iupac.org/S06101.html>
2. Shin, R. Y. C.; Teo, M. E.; Leong, W. K.; Vittal, J. J.; Yip, J. H. K.; Goh, L. Y.; Webster, R. D., *Organometallics* **2005**, *24*, 1483-1494.
3. Stubbe, J. A.; van der Donk, W. A., *Chem. Rev.* **1998**, *98*, 705-762.
4. Martin-Diaconescu, V.; Kennepohl, P., *J. Am. Chem. Soc.* **2007**, *129*, 3034-3035.
5. van Gastel, M.; Lubitz, W.; Lassmann, G.; Neese, F., *J. Am. Chem. Soc.* **2004**, *126*, 2237-2246.
6. *S-centered radicals*. ed.; John Wiley & Sons: Chichester, 1999; 'Vol.' p.
7. Walling, C.; Helmreich, W., *J. Am. Chem. Soc.* **1958**, *81*, 1144-1148.
8. J.E.Huheey, *Inorganic chemistry*. 3rd ed.; Harper & Row: New York, 1983; 'Vol.' p.
9. Ichinose, Y.; Oshima, K.; Utimoto, K., *Chem. Lett.* **1988**, 669-672.
10. Lalevee, J.; Allonas, X.; Fouassier, J. P., *J. Org. Chem.* **2006**, *71*, 9723-9727.
11. Chatgililoglu, C.; Ferreri, C.; Ballestri, M.; Mulazzani, Q. G.; Landi, L., *J. Am. Chem. Soc.* **2000**, *122*, 4593-4601.
12. <http://www.ncbi.nlm.nih.gov/books/bv.fcgi?rid=stryer.figgrp.3506>
13. Kimura, S.; Bill, E.; Bothe, E.; Weyhermuller, T.; Wieghardt, K., *J. Am. Chem. Soc.* **2001**, *123*, 6025-6039.
14. Ghosh, P.; Bill, E.; Weyhermuller, T.; Neese, F.; Wieghardt, K., *J Am Chem Soc* **2003**, *125*, 1293-1308.
15. Herebian, D.; Bothe, E.; Bill, E.; Weyhermuller, T.; Wieghardt, K., *J. Am. Chem. Soc.* **2001**, *123*, 10012-10023.
16. Hsieh, C. H.; Hsu, I. J.; Lee, C. M.; Ke, S. C.; Wang, T. Y.; Lee, G. H.; Wang, Y.; Chen, J. M.; Lee, J. F.; Liaw, W. F., *Inorg. Chem.* **2003**, *42*, 3925-3933.
17. Treichel, P. M.; Rosenhein, L. D., *Inorg. Chem.* **1984**, *23*, 4018-4022.
18. Albela, B.; Bothe, E.; Brosch, O.; Mochizuki, K.; Weyhermuller, T.; Wieghardt, K., *Inorg. Chem.* **1999**, *38*, 5131-5138.

19. Grapperhaus, C. A.; Poturovic, S., *Inorg. Chem.* **2004**, *43*, 3292-3298.
20. Poturovic, S.; Mashuta, M. S.; Grapperhaus, C. A., *Angew. Chem. Int. Edit.* **2005**, *44*, 1883-1887.
21. Grapperhaus, C. A.; Poturovic, S.; Mashuta, M. S., *Inorg. Chem.* **2002**, *41*, 4309-4311.
22. Gordon, A. J., *The Chemistry Companion*. ed.; John Wiley and Sons Inc.: Canada,, 1972
23. Dilworth, J. R.; Zheng, Y. F.; Lu, S. F.; Wu, Q. J., *Transition. Met. Chem.* **1992**, *17*, 364-368.
24. Grapperhaus, C. A.; Poturovic, S.; Mashuta, M. S., *Inorg. Chem.* **2005**, *44*, 8185-8187.
25. Farmer, P. J.; Reibenspies, J. H.; Lindahl, P. A.; Darensbourg, M. Y., *J. Am. Chem. Soc.* **1993**, *115*, 4665-4674.
26. Venturelli, A.; Rauchfuss, T. B.; Verma, A. K., *Inorg. Chem.* **1997**, *36*, 1360-1365.
27. Matsumoto, K.; Sugiyama, H., *Acc. Chem. Res.* **2002**, *35*, 915-926.
28. Wang, K.; Stiefel, E. I., *Science* **2001**, *291*, 106-109.
29. Harrison, D. J.; Nguyen, N.; Lough, A. J.; Fekl, U., *J. Am. Chem. Soc.* **2006**, *128*, 11026-11027.
30. John J. Manura and David J. Manura Isotope Distribution Calculator and Mass Spec Plotter. <http://www2.sisweb.com/mstools/isotope.htm>
31. Bell, H. M. *NMR Simulator*, 2004.
32. Dilworth, J. R.; Lu, C. Z.; Miller, J. R.; Zheng, Y. F., *J. Chem. Soc. Dalton Trans.* **1995**, 1957-1964.
33. Jia, G. C.; Rheingold, A. L.; Haggerty, B. S.; Meek, D. W., *Inorg. Chem.* **1992**, *31*, 900-904.
34. Nilges, M. J. *Simpow6*.
35. Que, L., *Physical Methods in Bioinorganic Chemistry: Spectroscopy and Magnetism*. ed.; University Science books: Sausalito, CA 94965,
36. Taylor, C. P. S., *Biochim. Biophys. Acta.* **1977**, *491*, 137-149.
37. SMART (v.5.628) Madison, WI; Bruker Advanced X-ray Solutions, Inc.: 2002.
38. SMART (v.6.36) Madison, WI; Bruker Advanced X-ray Solutions, Inc.: 2002.

39. Sheldrick, G.M. *SADABS* (v2.02), Gottingen, Germany; University Gottingen: 2001.
40. Sheldrick, G.M. *SHELXS-90*, A46; Acta Crystallogr.: 1990.
41. Sheldrick, G.M. *SHELXL-97*, Gottingen, Germany; University Gottingen: 1997.
42. *SHELXTL* (v.6.12) Madison, WI; Bruker Advanced X-ray Solutions, Inc.: 2001.
43. Sellmann, D.; Prakash, R.; Heinemann, F. W., *Eur. J. Inorg. Chem.* **2004**, 4291-4299.
44. Sellmann, D.; Prakash, R.; Heinemann, F. W.; Moll, M.; Klimowicz, M., *Angew. Chem. Int. Edit.* **2004**, *43*, 1877-1880.
45. Sellmann, D.; Shaban, S. Y.; Heinemann, F. W., *Eur. J. Inorg. Chem.* **2004**, 4591-4601.
46. Sellmann, D.; Shaban, S. Y.; Rosler, A.; Heinemann, F. W., *Inorg. Chim. Acta.* **2005**, *358*, 1798-1806.
47. Farrugia, L. J., *J. Appl. Crystallogr* **1997**, *30*, 565.
48. Grapperhaus, C. A.; Kozlowski, P. M.; Kumar, D.; Frye, H. N.; Venna, B. K.; Poturovic, S., *Angew. Chem. Int. Edit.* **2007**, 4085-4088.
49. Bruice, Y. P., *Organic Chemistry*. ed.; Prentice Hall: New Jersey 07458, 2001
50. Magistrato, A.; Maurer, P.; Fassler, T.; Rothlisberger, U., *J. Phys. Chem. A.* **2004**, *108*, 2008-2013.
51. Nantz, M. H.; Radisson, X.; Fuchs, P. L., *Synth. Commun.* **1987**, *17*, 55-69.

APPENDIX

List of Appendices

APPENDIX		PAGE
A	Tables and Figure for Crystallographic Data.....	54
B	Electrochemistry	61
C	UV-visible Spectroscopy	67
D	EPR Spectroscopy.....	71
E	NMR Spectroscopy.....	74
F	Mass Spectroscopy.....	78

APPENDIX A

Tables and Figure for Crystallographic Data

APPENDIX		PAGE
A-1	Experimental data for the X-ray crystal structure of 2a	55
A-2	Bond lengths (Å) and bond angles for 2a	56
A-3	X-ray crystal structure of 2a with full co-ordinates.....	60

Table A-1. Experimental data for the X-ray crystal structure of **2a**.

Empirical formula	C ₅₆ H ₄₆ Br P ₃ Ru S ₃ • 0.75 ClC ₆ H ₅
Formula weight	1173.41
Space group	P2 ₁ /c
a, Å	10.2565(9)
b, Å	13.2338(12)
c, Å	38.325(3)
β, deg	93.3960(10)°.
Volume, Å ³	5192.8(8) Å ³
Z	4
Density, Mg/m ³	1.501
Absorption coefficient	1.364 mm ⁻¹
Absorption correction	SADABS
Temperature	100(2) K
Final R indices [I>2σ(I)]	R1 = 0.0504, wR2 = 0.1164
R indices (all data)	R1 = 0.0646, wR2 = 0.1215

Table A-2. Bond lengths [Å] and bond angles [°] for **2a**.

Ru(1)-P(1)	2.3290(9)	C(17)-C(18)	1.393(6)
Ru(1)-S(3)	2.3365(9)	C(17)-H(17)	0.9300
Ru(1)-P(3)	2.3648(9)	C(18)-H(18)	0.9300
Ru(1)-S(2)	2.3749(9)	C(19)-C(20)	1.386(5)
Ru(1)-S(1)	2.3856(9)	C(19)-C(24)	1.387(5)
Ru(1)-P(2)	2.3965(10)	C(20)-C(21)	1.403(5)
S(1)-C(1)	1.751(4)	C(21)-C(22)	1.381(5)
S(2)-C(19)	1.787(4)	C(21)-H(21)	0.9300
S(2)-C(55)	1.836(4)	C(22)-C(23)	1.385(6)
S(3)-C(37)	1.805(4)	C(22)-H(22)	0.9300
S(3)-C(56)	1.843(4)	C(23)-C(24)	1.388(5)
P(1)-C(2)	1.818(4)	C(23)-H(23)	0.9300
P(1)-C(7)	1.834(4)	C(24)-H(24)	0.9300
P(1)-C(13)	1.846(4)	C(25)-C(30)	1.397(5)
P(2)-C(20)	1.829(4)	C(25)-C(26)	1.402(5)
P(2)-C(25)	1.832(4)	C(26)-C(27)	1.390(6)
P(2)-C(31)	1.835(4)	C(26)-H(26)	0.9300
P(3)-C(42)	1.822(4)	C(27)-C(28)	1.388(6)
P(3)-C(43)	1.834(4)	C(27)-H(27)	0.9300
P(3)-C(49)	1.836(4)	C(28)-C(29)	1.394(6)
C(1)-C(2)	1.397(5)	C(28)-H(28)	0.9300
C(1)-C(6)	1.409(5)	C(29)-C(30)	1.388(6)
C(2)-C(3)	1.404(5)	C(29)-H(29)	0.9300
C(3)-C(4)	1.372(6)	C(30)-H(30)	0.9300
C(3)-H(3)	0.9300	C(31)-C(36)	1.393(5)
C(4)-C(5)	1.391(6)	C(31)-C(32)	1.396(5)
C(4)-H(4)	0.9300	C(32)-C(33)	1.378(6)
C(5)-C(6)	1.377(6)	C(32)-H(32)	0.9300
C(5)-H(5)	0.9300	C(33)-C(34)	1.384(6)
C(6)-H(6)	0.9300	C(33)-H(33)	0.9300
C(7)-C(8)	1.398(5)	C(34)-C(35)	1.374(6)
C(7)-C(12)	1.400(5)	C(34)-H(34)	0.9300
C(8)-C(9)	1.386(5)	C(35)-C(36)	1.389(6)
C(8)-H(8)	0.9300	C(35)-H(35)	0.9300
C(9)-C(10)	1.384(6)	C(36)-H(36)	0.9300
C(9)-H(9)	0.9300	C(37)-C(42)	1.391(5)
C(10)-C(11)	1.386(6)	C(37)-C(38)	1.400(5)
C(10)-H(10)	0.9300	C(38)-C(39)	1.386(5)
C(11)-C(12)	1.392(5)	C(38)-H(38)	0.9300
C(11)-H(11)	0.9300	C(39)-C(40)	1.389(6)
C(12)-H(12)	0.9300	C(39)-H(39)	0.9300
C(13)-C(14)	1.397(5)	C(40)-C(41)	1.390(5)
C(13)-C(18)	1.398(5)	C(40)-H(40)	0.9300
C(14)-C(15)	1.390(5)	C(41)-C(42)	1.406(5)
C(14)-H(14)	0.9300	C(41)-H(41)	0.9300
C(15)-C(16)	1.383(6)	C(43)-C(48)	1.391(5)
C(15)-H(15)	0.9300	C(43)-C(44)	1.395(5)
C(16)-C(17)	1.379(6)	C(44)-C(45)	1.381(5)
C(16)-H(16)	0.9300	C(44)-H(44)	0.9300
C(45)-C(46)	1.374(6)	C(37)-S(3)-Ru(1)	107.40(12)
C(45)-H(45)	0.9300	C(56)-S(3)-Ru(1)	103.59(12)

C(46)-C(47)	1.385(6)	C(2)-P(1)-C(7)	106.91(17)
C(46)-H(46)	0.9300	C(2)-P(1)-C(13)	101.48(17)
C(47)-C(48)	1.391(6)	C(7)-P(1)-C(13)	99.85(16)
C(47)-H(47)	0.9300	C(2)-P(1)-Ru(1)	107.10(12)
C(48)-H(48)	0.9300	C(7)-P(1)-Ru(1)	117.70(12)
C(49)-C(54)	1.391(5)	C(13)-P(1)-Ru(1)	121.95(12)
C(49)-C(50)	1.400(5)	C(20)-P(2)-C(25)	99.36(16)
C(50)-C(51)	1.384(5)	C(20)-P(2)-C(31)	102.23(16)
C(50)-H(50)	0.9300	C(25)-P(2)-C(31)	102.07(17)
C(51)-C(52)	1.376(6)	C(20)-P(2)-Ru(1)	105.79(12)
C(51)-H(51)	0.9300	C(25)-P(2)-Ru(1)	127.03(12)
C(52)-C(53)	1.392(6)	C(31)-P(2)-Ru(1)	116.56(12)
C(52)-H(52)	0.9300	C(42)-P(3)-C(43)	106.78(17)
C(53)-C(54)	1.391(5)	C(42)-P(3)-C(49)	101.81(16)
C(53)-H(53)	0.9300	C(43)-P(3)-C(49)	103.95(17)
C(54)-H(54)	0.9300	C(42)-P(3)-Ru(1)	107.39(12)
C(55)-C(56)	1.510(5)	C(43)-P(3)-Ru(1)	123.09(12)
C(55)-H(55A)	0.9700	C(49)-P(3)-Ru(1)	111.75(12)
C(55)-H(55B)	0.9700	C(2)-C(1)-C(6)	118.7(3)
C(56)-H(56A)	0.9700	C(2)-C(1)-S(1)	122.8(3)
C(56)-H(56B)	0.9700	C(6)-C(1)-S(1)	118.5(3)
Cl(1)-C(60)	1.769(7)	C(1)-C(2)-C(3)	119.5(3)
C(60)-C(61)	1.316(9)	C(1)-C(2)-P(1)	118.3(3)
C(60)-C(65)	1.366(8)	C(3)-C(2)-P(1)	122.1(3)
C(61)-C(62)	1.393(9)	C(4)-C(3)-C(2)	121.2(4)
C(61)-H(61)	0.9300	C(4)-C(3)-H(3)	119.4
C(62)-C(63)	1.321(8)	C(2)-C(3)-H(3)	119.4
C(62)-H(62)	0.9300	C(3)-C(4)-C(5)	119.2(4)
C(63)-C(64)	1.417(9)	C(3)-C(4)-H(4)	120.4
C(63)-H(63)	0.9300	C(5)-C(4)-H(4)	120.4
C(64)-C(65)	1.352(9)	C(6)-C(5)-C(4)	120.8(4)
C(64)-H(64)	0.9300	C(6)-C(5)-H(5)	119.6
C(65)-H(65)	0.9300	C(4)-C(5)-H(5)	119.6
P(1)-Ru(1)-S(3)	99.28(3)	C(5)-C(6)-C(1)	120.5(4)
P(1)-Ru(1)-P(3)	93.62(3)	C(5)-C(6)-H(6)	119.7
S(3)-Ru(1)-P(3)	85.55(3)	C(1)-C(6)-H(6)	119.7
P(1)-Ru(1)-S(2)	172.87(3)	C(8)-C(7)-C(12)	118.1(3)
S(3)-Ru(1)-S(2)	87.71(3)	C(8)-C(7)-P(1)	118.4(3)
P(3)-Ru(1)-S(2)	85.48(3)	C(12)-C(7)-P(1)	123.5(3)
P(1)-Ru(1)-S(1)	85.88(3)	C(9)-C(8)-C(7)	121.1(4)
S(3)-Ru(1)-S(1)	173.73(3)	C(9)-C(8)-H(8)	119.4
P(3)-Ru(1)-S(1)	90.59(3)	C(7)-C(8)-H(8)	119.4
S(2)-Ru(1)-S(1)	87.06(3)	C(10)-C(9)-C(8)	120.0(4)
P(1)-Ru(1)-P(2)	97.56(3)	C(10)-C(9)-H(9)	120.0
S(3)-Ru(1)-P(2)	93.12(3)	C(8)-C(9)-H(9)	120.0
P(3)-Ru(1)-P(2)	168.81(3)	C(9)-C(10)-C(11)	119.9(4)
S(2)-Ru(1)-P(2)	83.36(3)	C(9)-C(10)-H(10)	120.0
S(1)-Ru(1)-P(2)	89.70(3)	C(11)-C(10)-H(10)	120.0
C(1)-S(1)-Ru(1)	105.77(13)	C(10)-C(11)-C(12)	120.1(4)
C(19)-S(2)-C(55)	103.00(17)	C(10)-C(11)-H(11)	119.9
C(19)-S(2)-Ru(1)	108.13(12)	C(12)-C(11)-H(11)	119.9
C(55)-S(2)-Ru(1)	104.52(12)	C(11)-C(12)-C(7)	120.7(4)
C(37)-S(3)-C(56)	99.79(17)	C(11)-C(12)-H(12)	119.7
C(7)-C(12)-H(12)	119.7	C(36)-C(31)-P(2)	122.8(3)
C(14)-C(13)-C(18)	118.7(3)	C(32)-C(31)-P(2)	118.8(3)
C(14)-C(13)-P(1)	118.8(3)	C(33)-C(32)-C(31)	120.2(4)

C(18)-C(13)-P(1)	122.5(3)	C(33)-C(32)-H(32)	119.9
C(15)-C(14)-C(13)	120.8(4)	C(31)-C(32)-H(32)	119.9
C(15)-C(14)-H(14)	119.6	C(32)-C(33)-C(34)	121.0(4)
C(13)-C(14)-H(14)	119.6	C(32)-C(33)-H(33)	119.5
C(16)-C(15)-C(14)	120.0(4)	C(34)-C(33)-H(33)	119.5
C(16)-C(15)-H(15)	120.0	C(35)-C(34)-C(33)	119.4(4)
C(14)-C(15)-H(15)	120.0	C(35)-C(34)-H(34)	120.3
C(17)-C(16)-C(15)	119.7(4)	C(33)-C(34)-H(34)	120.3
C(17)-C(16)-H(16)	120.2	C(34)-C(35)-C(36)	120.1(4)
C(15)-C(16)-H(16)	120.2	C(34)-C(35)-H(35)	119.9
C(16)-C(17)-C(18)	120.9(4)	C(36)-C(35)-H(35)	119.9
C(16)-C(17)-H(17)	119.5	C(35)-C(36)-C(31)	120.9(4)
C(18)-C(17)-H(17)	119.5	C(35)-C(36)-H(36)	119.5
C(17)-C(18)-C(13)	119.8(4)	C(31)-C(36)-H(36)	119.5
C(17)-C(18)-H(18)	120.1	C(42)-C(37)-C(38)	121.0(3)
C(13)-C(18)-H(18)	120.1	C(42)-C(37)-S(3)	121.3(3)
C(20)-C(19)-C(24)	122.0(3)	C(38)-C(37)-S(3)	117.7(3)
C(20)-C(19)-S(2)	119.8(3)	C(39)-C(38)-C(37)	119.9(4)
C(24)-C(19)-S(2)	117.9(3)	C(39)-C(38)-H(38)	120.1
C(19)-C(20)-C(21)	118.3(3)	C(37)-C(38)-H(38)	120.1
C(19)-C(20)-P(2)	119.1(3)	C(38)-C(39)-C(40)	119.9(3)
C(21)-C(20)-P(2)	122.6(3)	C(38)-C(39)-H(39)	120.1
C(22)-C(21)-C(20)	120.2(4)	C(40)-C(39)-H(39)	120.1
C(22)-C(21)-H(21)	119.9	C(39)-C(40)-C(41)	120.2(3)
C(20)-C(21)-H(21)	119.9	C(39)-C(40)-H(40)	119.9
C(21)-C(22)-C(23)	120.4(4)	C(41)-C(40)-H(40)	119.9
C(21)-C(22)-H(22)	119.8	C(40)-C(41)-C(42)	120.7(3)
C(23)-C(22)-H(22)	119.8	C(40)-C(41)-H(41)	119.7
C(22)-C(23)-C(24)	120.4(3)	C(42)-C(41)-H(41)	119.7
C(22)-C(23)-H(23)	119.8	C(37)-C(42)-C(41)	118.3(3)
C(24)-C(23)-H(23)	119.8	C(37)-C(42)-P(3)	118.3(3)
C(19)-C(24)-C(23)	118.7(3)	C(41)-C(42)-P(3)	123.4(3)
C(19)-C(24)-H(24)	120.7	C(48)-C(43)-C(44)	118.2(3)
C(23)-C(24)-H(24)	120.7	C(48)-C(43)-P(3)	117.9(3)
C(30)-C(25)-C(26)	118.8(4)	C(44)-C(43)-P(3)	123.9(3)
C(30)-C(25)-P(2)	119.4(3)	C(45)-C(44)-C(43)	121.1(4)
C(26)-C(25)-P(2)	121.8(3)	C(45)-C(44)-H(44)	119.5
C(27)-C(26)-C(25)	120.3(4)	C(43)-C(44)-H(44)	119.5
C(27)-C(26)-H(26)	119.9	C(46)-C(45)-C(44)	120.4(4)
C(25)-C(26)-H(26)	119.9	C(46)-C(45)-H(45)	119.8
C(28)-C(27)-C(26)	120.5(4)	C(44)-C(45)-H(45)	119.8
C(28)-C(27)-H(27)	119.7	C(45)-C(46)-C(47)	119.4(4)
C(26)-C(27)-H(27)	119.7	C(45)-C(46)-H(46)	120.3
C(27)-C(28)-C(29)	119.5(4)	C(47)-C(46)-H(46)	120.3
C(27)-C(28)-H(28)	120.2	C(46)-C(47)-C(48)	120.5(4)
C(29)-C(28)-H(28)	120.2	C(46)-C(47)-H(47)	119.7
C(30)-C(29)-C(28)	120.1(4)	C(48)-C(47)-H(47)	119.7
C(30)-C(29)-H(29)	119.9	C(43)-C(48)-C(47)	120.3(4)
C(28)-C(29)-H(29)	119.9	C(43)-C(48)-H(48)	119.8
C(29)-C(30)-C(25)	120.8(4)	C(47)-C(48)-H(48)	119.8
C(29)-C(30)-H(30)	119.6	C(54)-C(49)-C(50)	118.2(3)
C(25)-C(30)-H(30)	119.6	C(54)-C(49)-P(3)	121.1(3)
C(36)-C(31)-C(32)	118.3(3)	C(50)-C(49)-P(3)	119.8(3)
C(51)-C(50)-C(49)	120.7(4)		
C(51)-C(50)-H(50)	119.7		
C(49)-C(50)-H(50)	119.7		

C(52)-C(51)-C(50)	120.5(4)
C(52)-C(51)-H(51)	119.7
C(50)-C(51)-H(51)	119.7
C(51)-C(52)-C(53)	119.7(4)
C(51)-C(52)-H(52)	120.1
C(53)-C(52)-H(52)	120.1
C(54)-C(53)-C(52)	119.6(4)
C(54)-C(53)-H(53)	120.2
C(52)-C(53)-H(53)	120.2
C(53)-C(54)-C(49)	121.1(4)
C(53)-C(54)-H(54)	119.5
C(49)-C(54)-H(54)	119.5
C(56)-C(55)-S(2)	114.0(3)
C(56)-C(55)-H(55A)	108.8
S(2)-C(55)-H(55A)	108.8
C(56)-C(55)-H(55B)	108.8
S(2)-C(55)-H(55B)	108.8
H(55A)-C(55)-H(55B)	107.7
C(55)-C(56)-S(3)	112.8(3)
C(55)-C(56)-H(56A)	109.0
S(3)-C(56)-H(56A)	109.0
C(55)-C(56)-H(56B)	109.0
S(3)-C(56)-H(56B)	109.0
H(56A)-C(56)-H(56B)	107.8
C(61)-C(60)-C(65)	122.6(6)
C(61)-C(60)-Cl(1)	119.8(5)
C(65)-C(60)-Cl(1)	117.6(5)
C(60)-C(61)-C(62)	119.3(6)
C(60)-C(61)-H(61)	120.3
C(62)-C(61)-H(61)	120.3
C(63)-C(62)-C(61)	121.0(6)
C(63)-C(62)-H(62)	119.5
C(61)-C(62)-H(62)	119.5
C(62)-C(63)-C(64)	118.2(6)
C(62)-C(63)-H(63)	120.9
C(64)-C(63)-H(63)	120.9
C(65)-C(64)-C(63)	120.8(6)
C(65)-C(64)-H(64)	119.6
C(63)-C(64)-H(64)	119.6
C(64)-C(65)-C(60)	117.9(6)
C(64)-C(65)-H(65)	121.0
C(60)-C(65)-H(65)	121.0

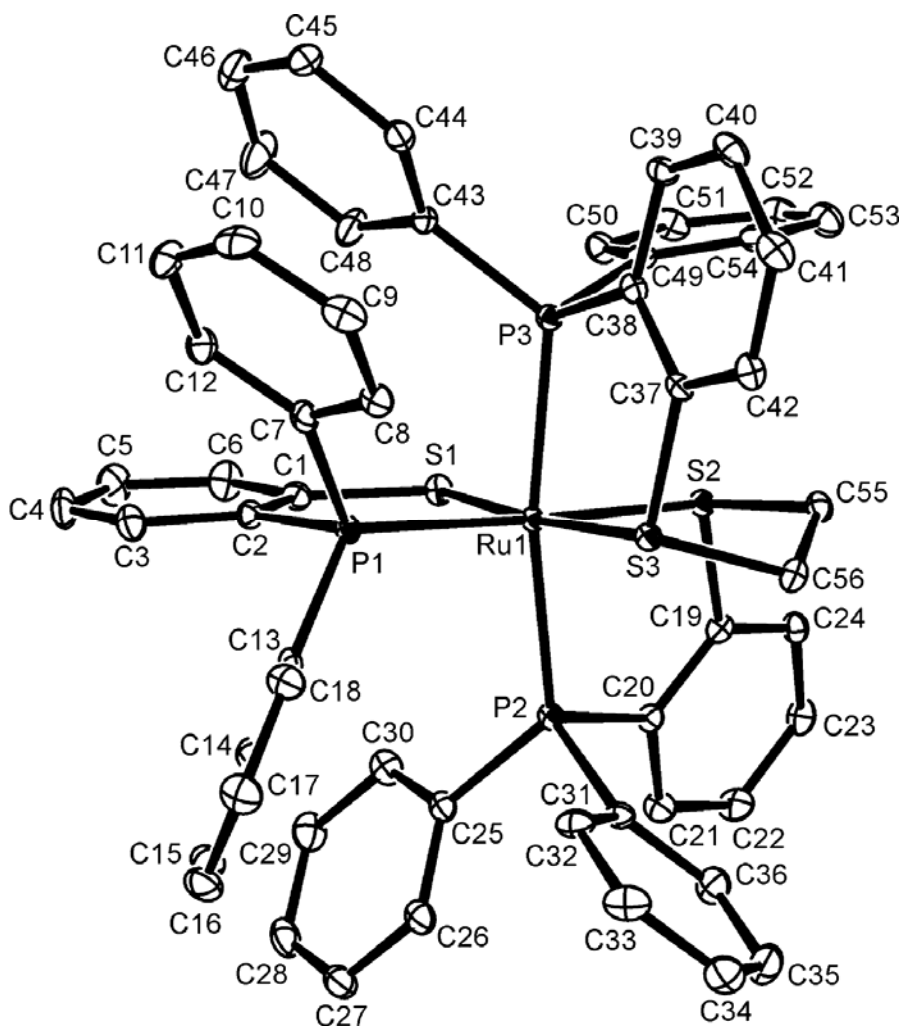


Figure A-3: An ORTEP diagram of the cation of **2a** with full atom labeling scheme.

Hydrogen atoms and solvent molecules are omitted for clarity.

APPENDIX B

Electrochemistry

APPENDIX		PAGE
B-1	Square wave voltammogram of 3a	62
B-2	Square wave voltammogram of 4a	62
B-3	Square wave voltammogram of 5a	63
B-4	Square wave voltammogram of 6a	63
B-5	Square wave voltammogram of 2a (Chemically generated).....	64
B-6	Square wave voltammogram of 3b	64
B-7	Square wave voltammogram of 4b	65
B-8	Square wave voltammogram of 5b	65
B-9	Square wave voltammogram of 6b	66

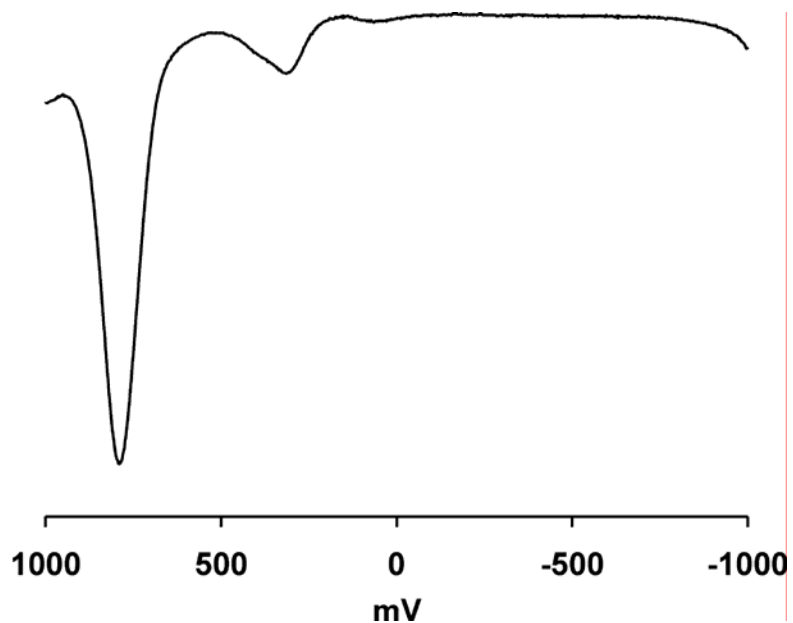


Figure B-1. Square wave voltammogram of **3a** in acetonitrile with 0.1M TBAHFP at -20 °C. Potentials referenced to Ag/AgCl.

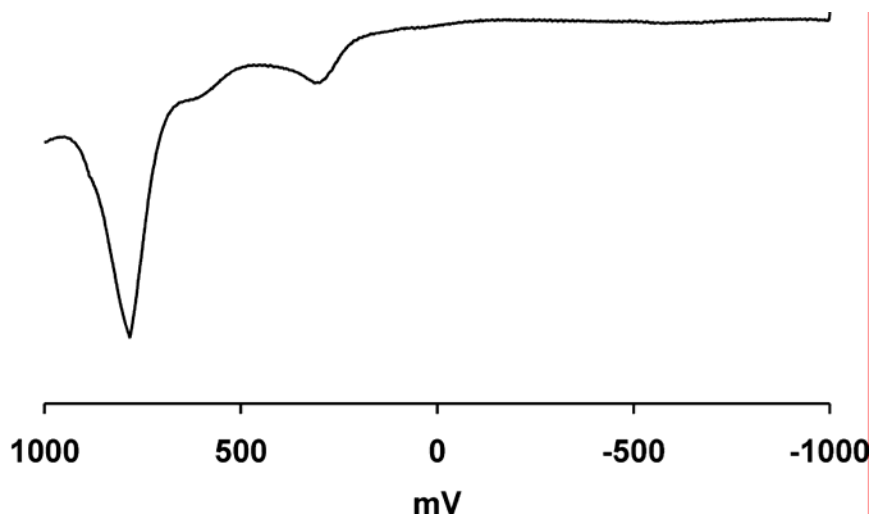


Figure B-2. Square wave voltammogram of **4a** in acetonitrile with 0.1M TBAHFP at -20 °C. Potentials referenced to Ag/AgCl.

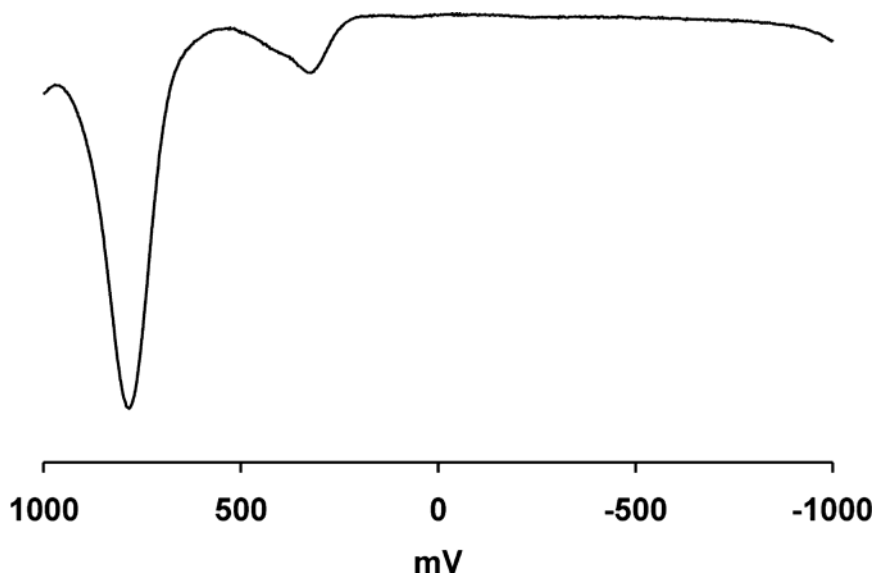


Figure B-3. Square wave voltammogram of **5a** in acetonitrile with 0.1M TBAHFP at -20°C. Potentials referenced to Ag/AgCl.

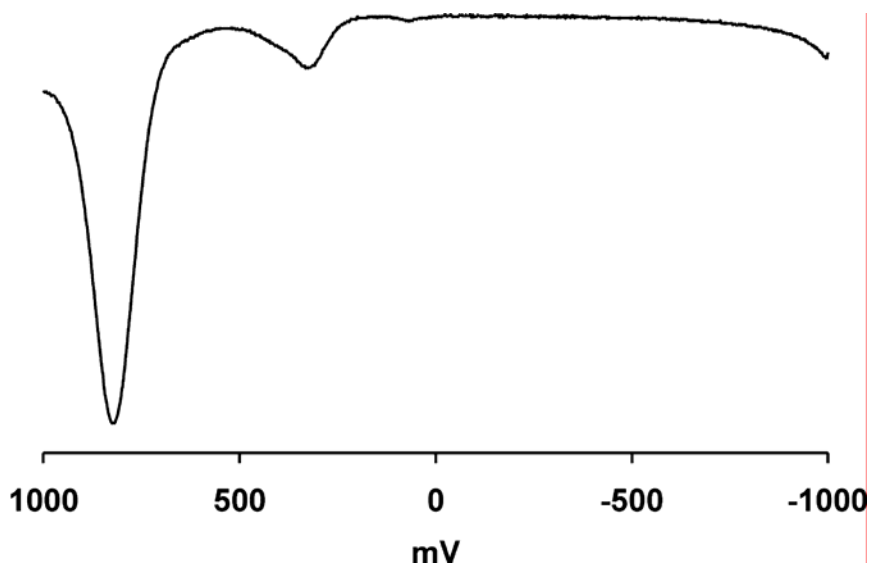


Figure B-4. Square wave voltammogram of **6a** in acetonitrile with 0.1M TBAHFP at -20 °C. Potentials referenced to Ag/AgCl.

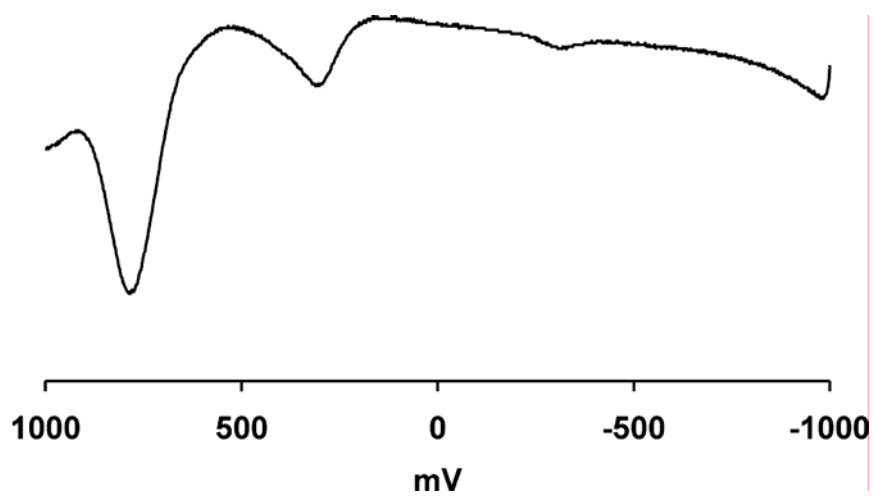


Figure B-5. Square wave voltammogram of **2a** (chemically generated) in acetonitrile with 0.1M TBAHFP at -20 °C. Potentials referenced to Ag/AgCl.

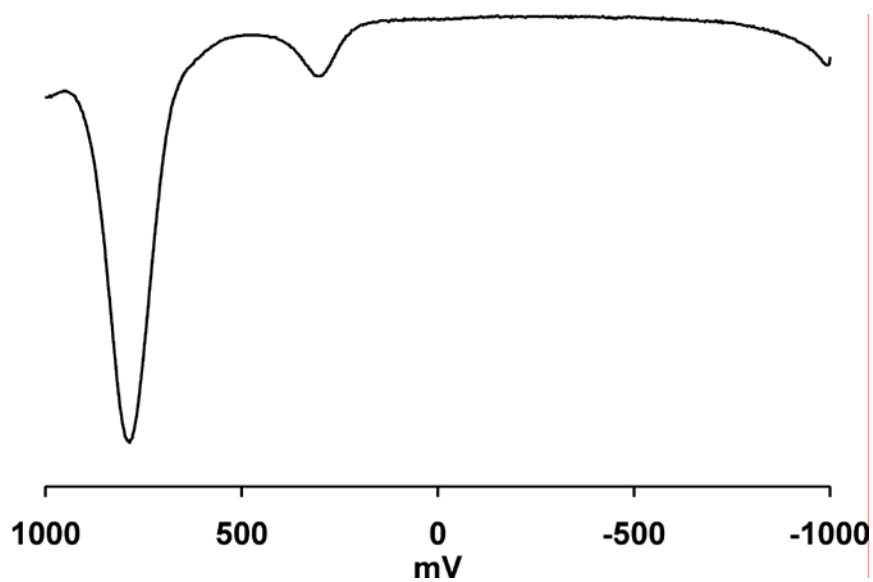


Figure B-6. Square wave voltammogram of **3b** in acetonitrile with 0.1M TBAHFP at -20 °C. Potentials referenced to Ag/AgCl.

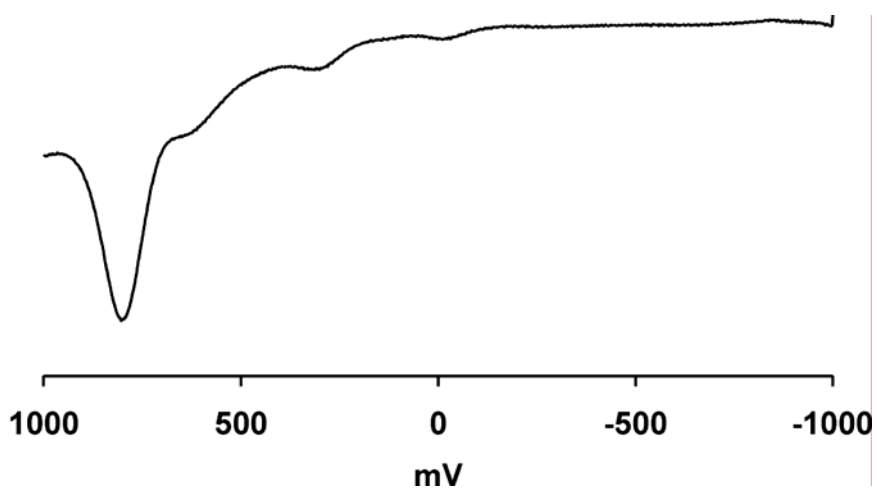


Figure B-7. Square wave voltammogram of **4b** in acetonitrile with 0.1M TBAHFP at -20 °C. Potentials referenced to Ag/AgCl.

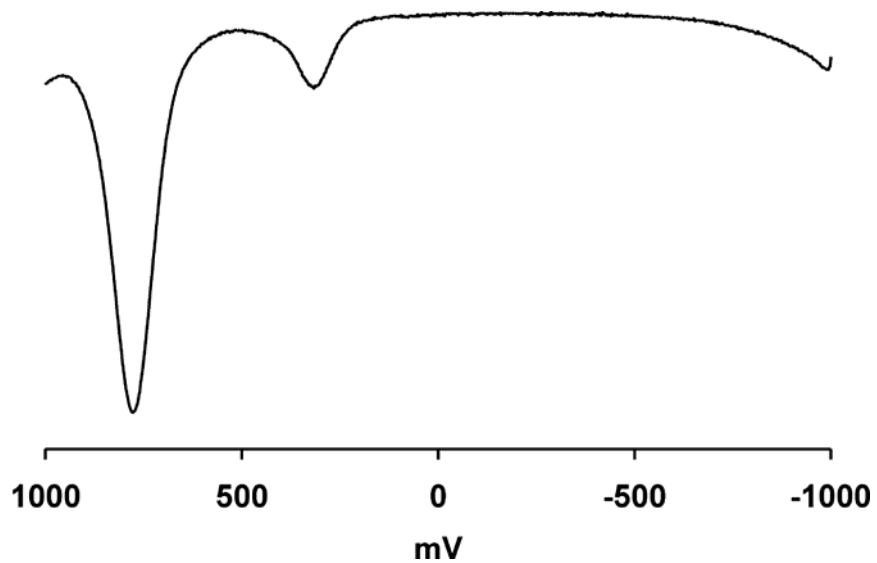


Figure B-8. Square wave voltammogram of **5b** in acetonitrile with 0.1M TBAHFP at -20 °C. Potentials referenced to Ag/AgCl.

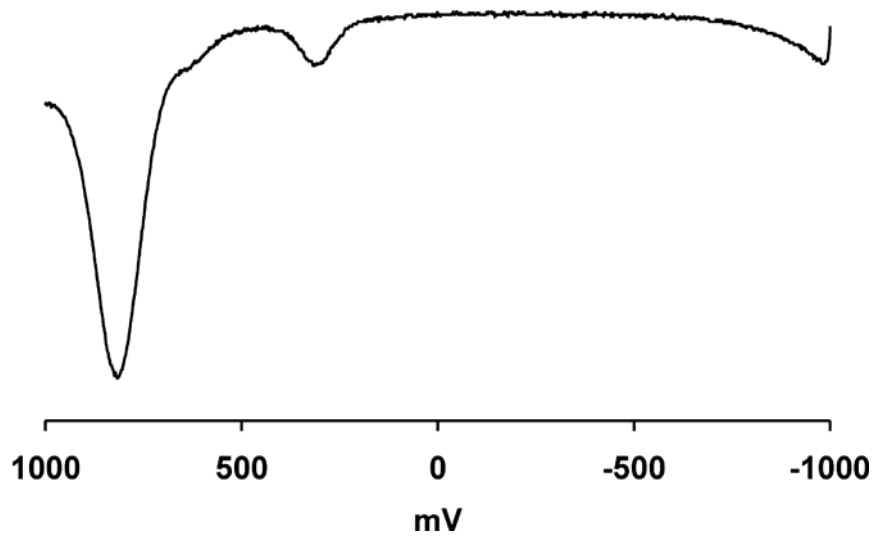


Figure B-9. Square wave voltammogram of **6b** in acetonitrile with 0.1M TBAHFP at -20 °C. Potentials referenced to Ag/AgCl.

APPENDIX C

UV-Visible Spectroscopy

APPENDIX		PAGE
C-1	Electronic spectra obtained during oxidation of 1b to 3a	68
C-2	Electronic spectra obtained during oxidation of 1b to 4a	68
C-3	Electronic spectra obtained during oxidation of 1b to 5a	69
C-4	Electronic spectra obtained during oxidation of 3a to 3b	69
C-5	Electronic spectra obtained during oxidation of 4a to 4b	70
C-6	Electronic spectra obtained during oxidation of 5a to 5b	70

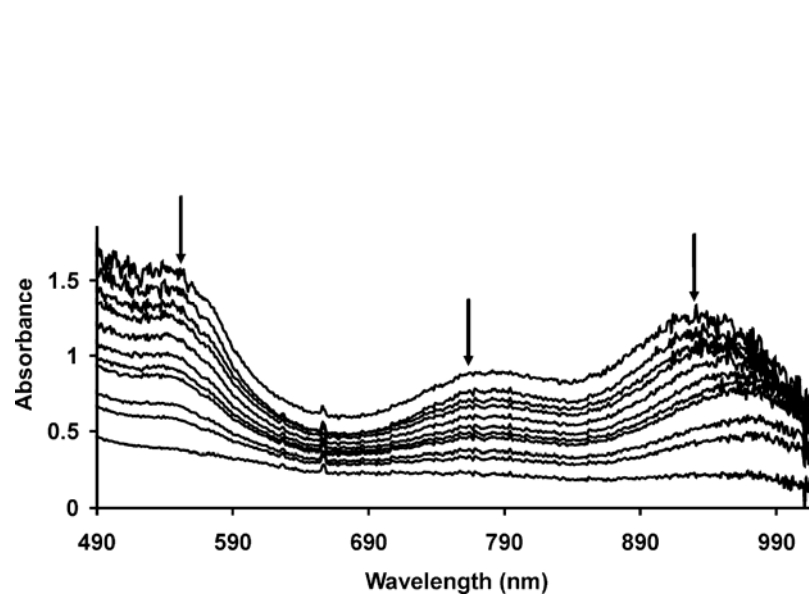


Figure C-1. Electronic spectra obtained during oxidation of **1b** to **3a**. Spectra were obtained approximately for every one tenth of electron equivalent in MeCN solution at $-20\text{ }^{\circ}\text{C}$.

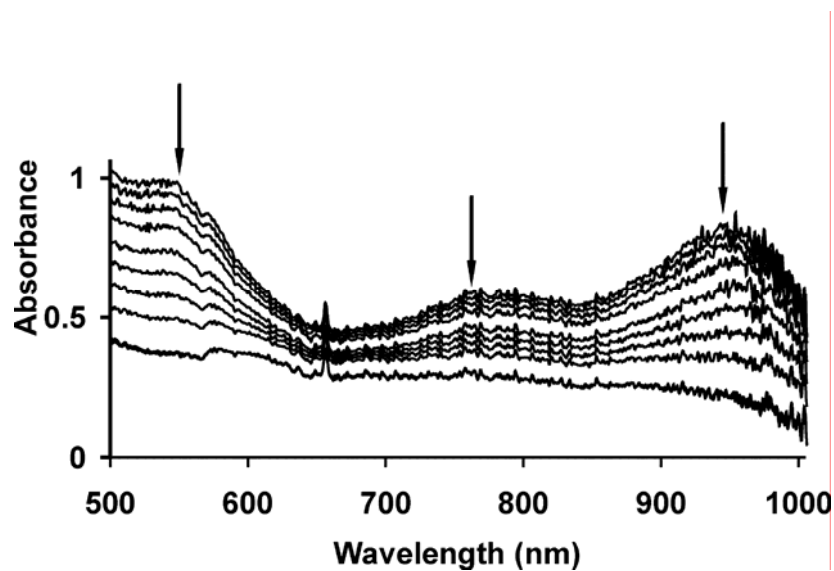


Figure C-2. Electronic spectra obtained during oxidation of **1b** to **4a**. Spectra were obtained approximately for every one tenth of electron equivalent in MeCN solution at $-20\text{ }^{\circ}\text{C}$.

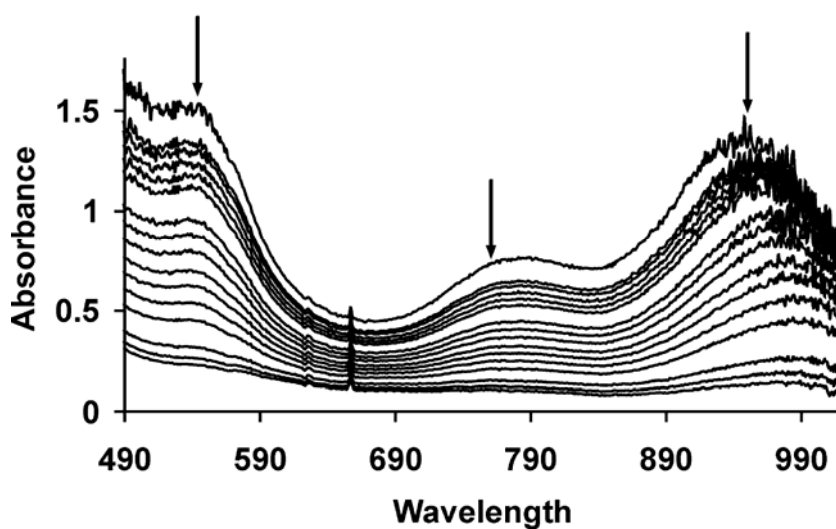


Figure C-3. Electronic spectra obtained during oxidation of **1b** to **5a**. Spectra were obtained approximately for every one tenth of electron equivalent in MeCN solution at $-20\text{ }^{\circ}\text{C}$.

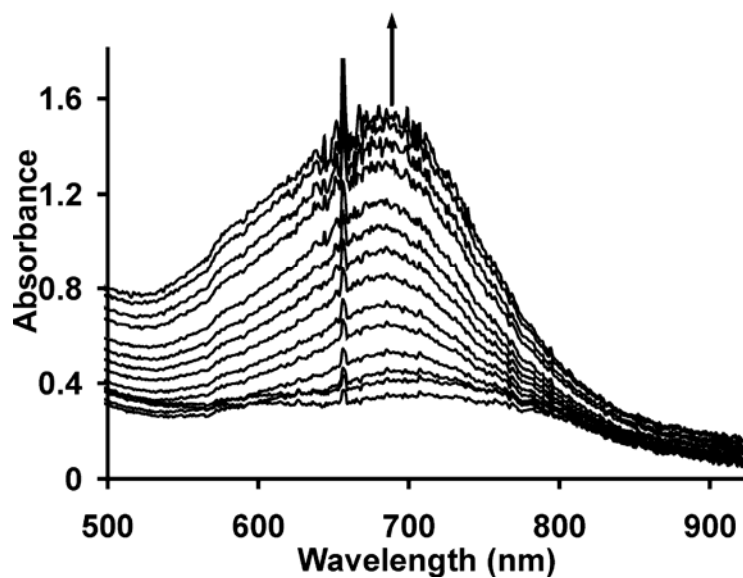


Figure C-4. Electronic spectra obtained during oxidation of **3a** to **3b**. Spectra were obtained approximately for every one tenth of electron equivalent in MeCN solution at $-20\text{ }^{\circ}\text{C}$.

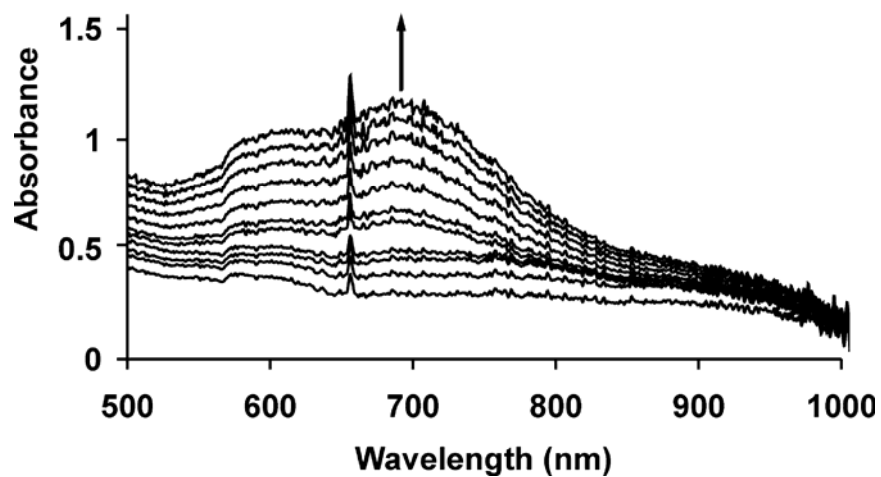


Figure C-5. Electronic spectra obtained during oxidation of **4a** to **4b**. Spectra were obtained approximately for every one tenth of electron equivalent in MeCN solution at $-20\text{ }^{\circ}\text{C}$.

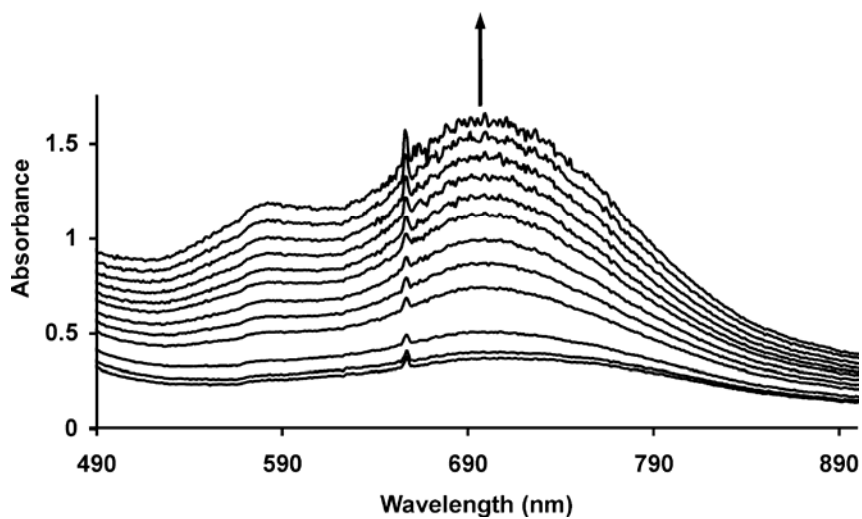


Figure C-6. Electronic spectra obtained during oxidation of **5a** to **5b**. Spectra were obtained approximately for every one tenth of electron equivalent in MeCN solution at $-20\text{ }^{\circ}\text{C}$.

APPENDIX D

EPR Spectroscopy

APPENDIX		PAGE
D-1	EPR spectrum of 3b	72
D-2	EPR spectrum of 4b	72
D-3	EPR spectrum of 5b	73
D-4	EPR spectrum of 6b	73

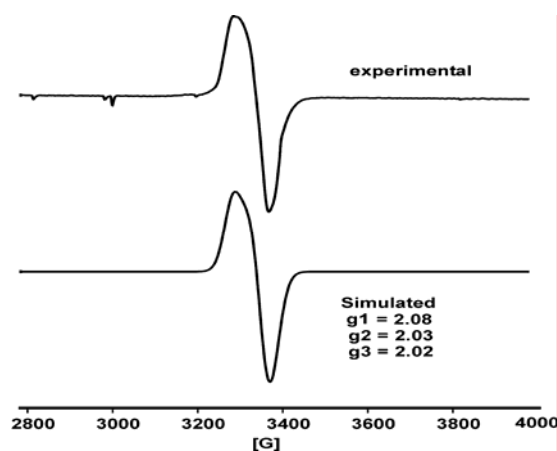


Figure D-1. EPR spectrum of **3b** at 77 K. Experimental Conditions: microwave frequency of 9.604674 GHz; microwave power 3.955 mW, modulation frequency 100 kHz, modulation amplitude of 3.350 G. Line widths for simulated spectrum: $W_x = 22$, $W_y = 19$, $W_z = 17$.

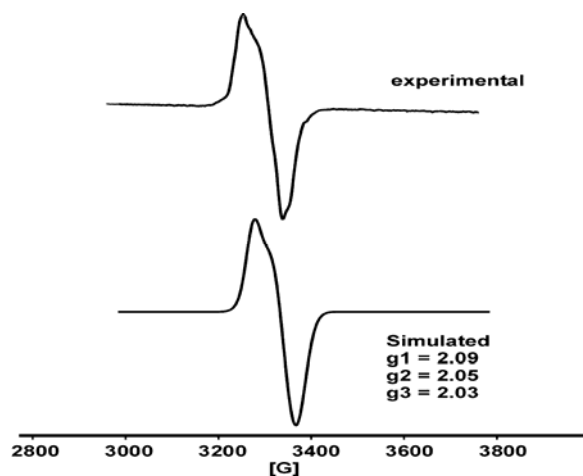


Figure D-2. EPR spectrum of **4b** at 77K. Experimental Conditions: microwave frequency of 9.604621 GHz; microwave power 4.014 mW, modulation frequency 100 kHz, modulation amplitude of 3.350 G. Line widths for simulated spectrum : $W_x = 22$, $W_y = 29$, $W_z = 27$.

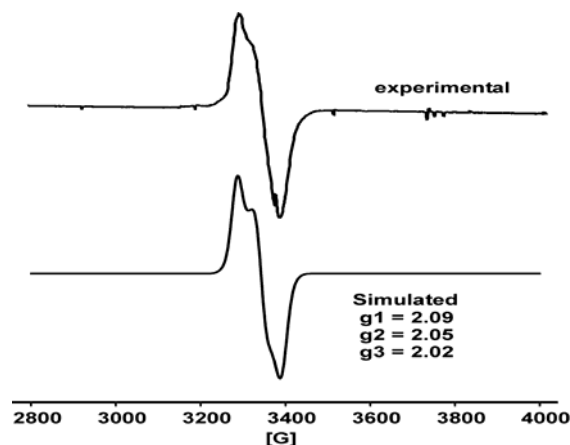


Figure D-3. EPR spectrum of **5b** at 77K. Experimental Conditions: microwave frequency of 9.605321 GHz; microwave power 4.024 mW, modulation frequency 100 kHz, modulation amplitude of 3.350G. Line widths for simulated spectrum: $W_x = 21$, $W_y = 20$, $W_z = 20$.

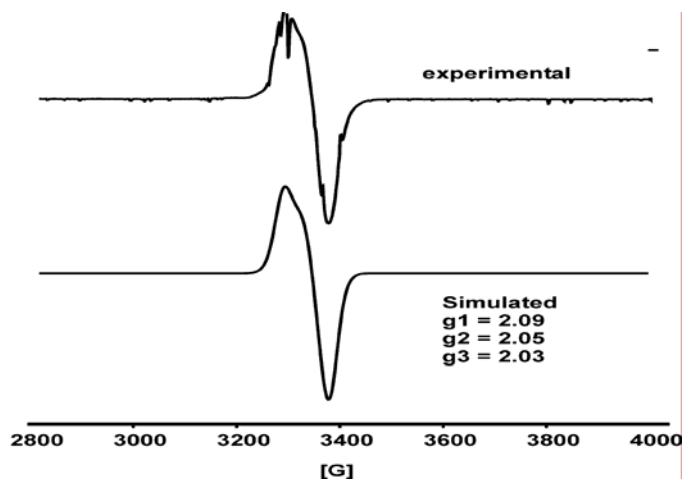


Figure D-4. EPR spectrum of **6b** at 77K. Experimental Conditions: microwave frequency of 9.603509 GHz; microwave power 2.012 mW, modulation frequency 100 kHz, modulation amplitude of 10 G. Line widths for simulated spectrum : $W_x = 22$, $W_y = 19$, $W_z = 17$.

APPENDIX E

NMR Spectroscopy

APPENDIX		PAGE
E-1	³¹ P NMR spectrum of 3a in deuterated acetonitrile.....	75
E-2	³¹ P NMR spectrum of 4a-I in deuterated acetonitrile.....	75
E-3	³¹ P NMR spectrum of 4a-II in deuterated acetonitrile	76
E-4	³¹ P NMR spectrum of 5a in deuterated acetonitrile.....	76
E-5	³¹ P NMR spectrum of 6a in deuterated acetonitrile.....	77

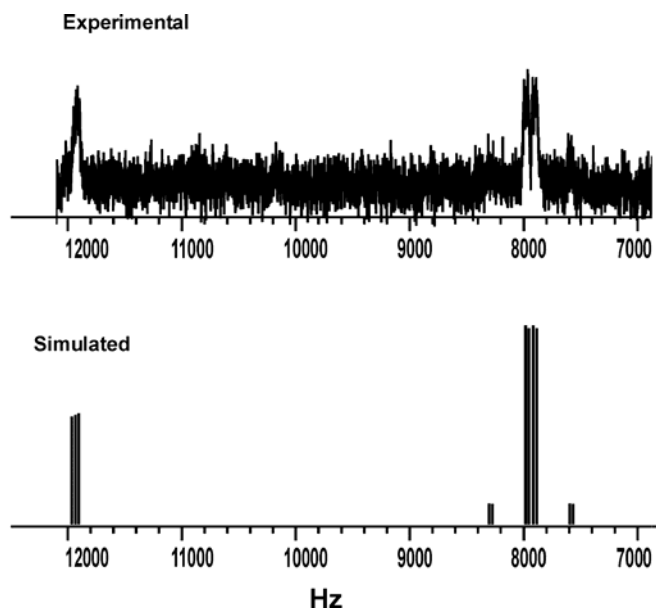


Figure E-1. ^{31}P NMR spectrum of **3a** in deuterated acetonitrile. NMR spectrum was simulated by using Freqint program.

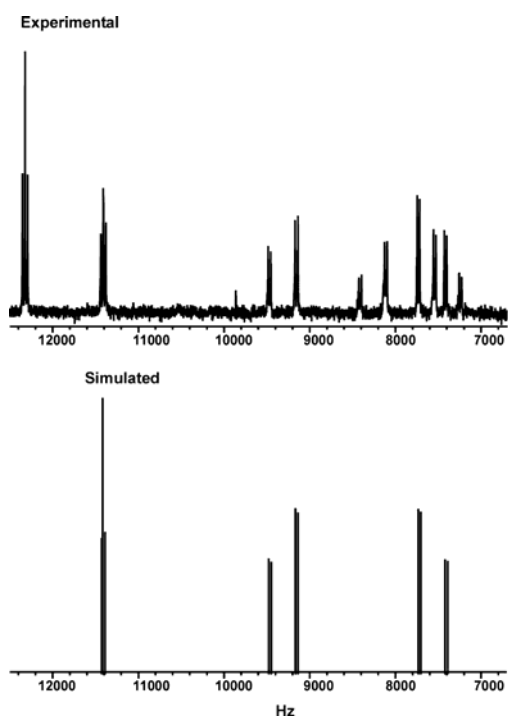


Figure E-2. ^{31}P NMR spectrum of **4a-I** in deuterated acetonitrile. NMR spectrum was simulated by using Freqint program.

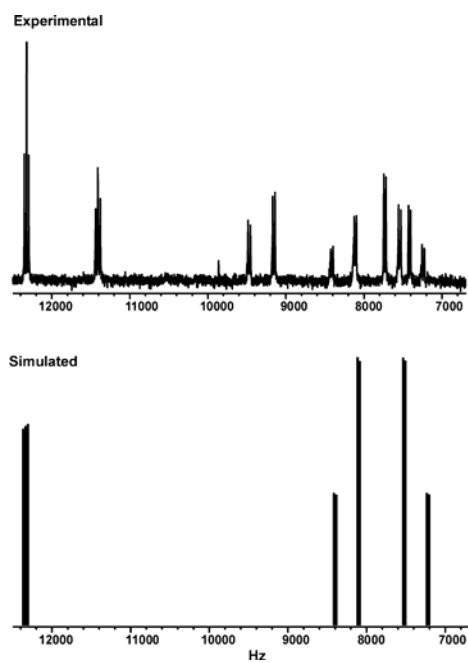


Figure E-3. ^{31}P NMR spectrum of **4a-II** in deuterated acetonitrile. NMR spectrum was simulated by using Freqaint program.

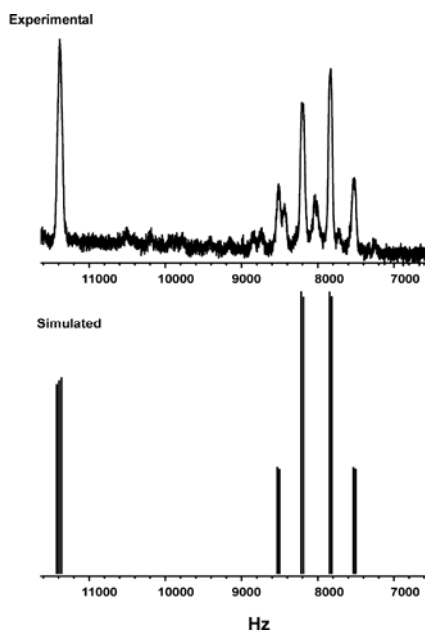


Figure E-4. ^{31}P NMR spectrum of **5a** in deuterated acetonitrile. NMR spectrum was simulated by using Freqaint program.

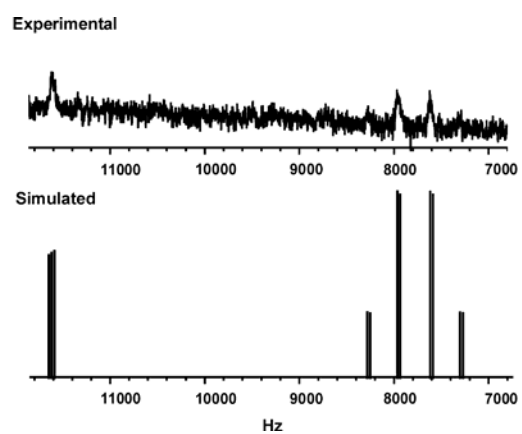


Figure E-5. ^{31}P NMR spectrum of **6a** in deuterated acetonitrile. NMR spectrum was simulated by using Freqint program

APPENDIX F

Mass spectroscopy

APPENDIX		PAGE
F-1	+ESI-MS of 3a in acetonitrile.....	79
F-2	+ESI-MS of 4a in acetonitrile.....	79
F-3	+ESI-MS of 5a in acetonitrile.....	80
F-4	+ESI-MS of 6a in acetonitrile.....	80
F-5	+ESI-MS of 2a (chemically generated) in CH ₃ CN.....	81

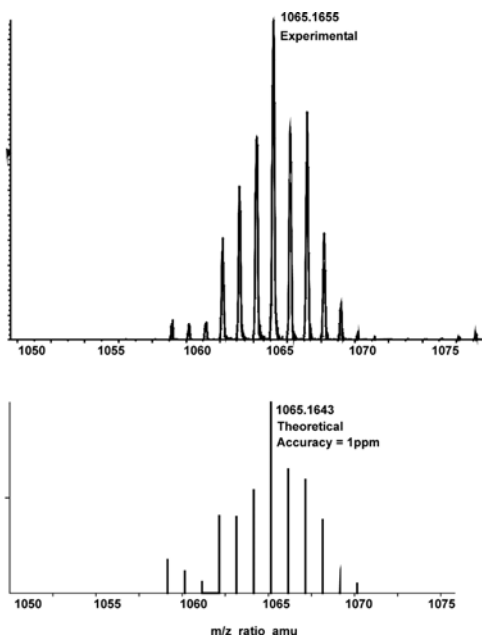


Figure F-1. +ESI-MS of **3a** in acetonitrile.

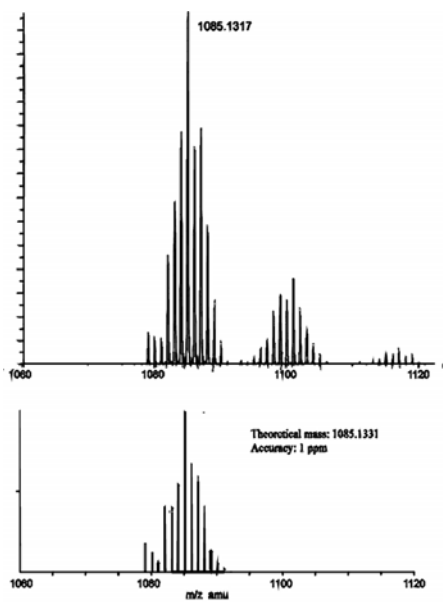


Figure F-2. +ESI-MS of **4a** in acetonitrile.

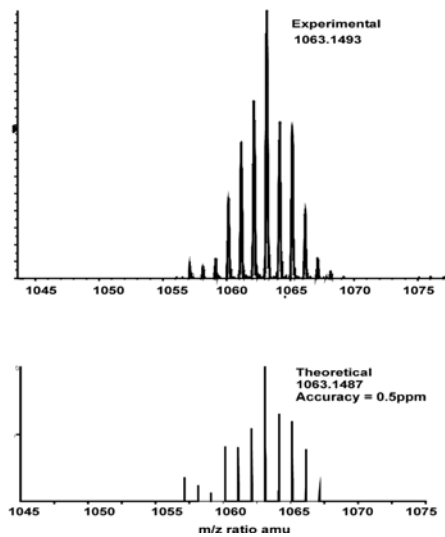


Figure F-3. +ESI-MS of **5a** in acetonitrile.

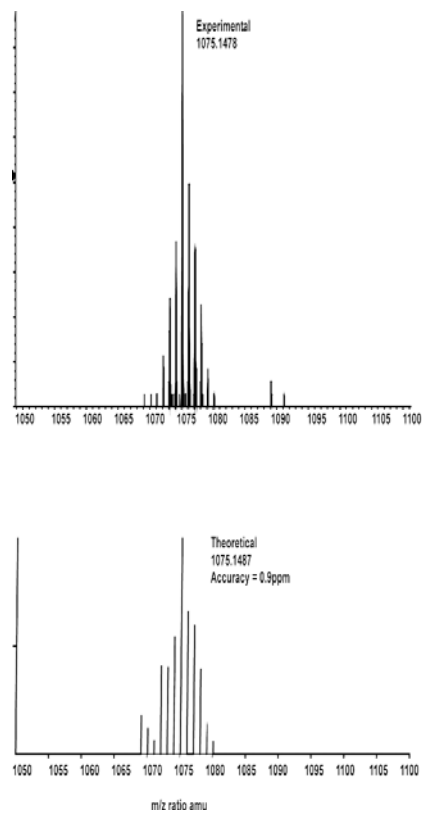


Figure F-4. +ESI-MS of **6a** in acetonitrile.

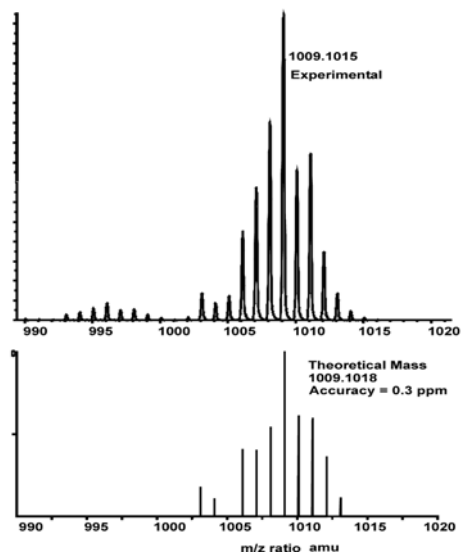


Figure F-5. +ESI-MS of **2a** (chemically generated) in acetonitrile.

CURRICULUM VITAE

NAME: Kiran B Venna

ADDRESS University Of Louisville
2320 South Brook Street
Louisville, KY, 40292

DOB Gudiwada, AP, India, September 23, 1974

EDUCATION
& TRAINING M.Sc., Chemistry
Acharya Nagarjuna University, Nagarjunanagar, AP, India.
1996-1998

M.S., Chemistry
University Of Louisville, Louisville, Ky
Louisville

PUBLICATIONS **Singlet Diradical Character of an Oxidized Ruthenium trithiolate: Electronic Structure and Reactivity.** Grapperhaus, C.A.; Kozlowski, P.M.; Kumar, D.; Frye, H.N.; Venna, K.B.; Poturovic, S. *Angewandte Chemie* **2007**.

Carbon-Sulfur Bond formation via Alkene Addition to an Oxidized Ruthenium-Thiolate. Grapperhaus, C.A.; Venna, K.B. Poturovic, S.; Mashuta, M.S. manuscript in preparation

PRESENTATIONS Venna, K.B.; Grapperhaus, C.A.; Mashuta, M.S., Poturovic, S.; Kozlowski, P.M. **Carbon-Sulfur Bond formation via Alkene Addition to an Oxidized Ruthenium-Thiolate.** 233rd ACS National Meeting, Chicago, IL, March, 25-29, 2007.

Venna, K.B.; Grapperhaus, C.A.; Mashuta, M.S.; Poturovic, S.; Kozlowski, P.M. **Carbon-Sulfur Bond formation via Alkene Addition to an Oxidized Ruthenium-Thiolate.** CERMACS 2007, Covington, KY, 2007.